Quantification in low-energy ion scattering

Elfrink, R.J.M.

Award date:
2001

Eindhoven University of Technology

Faculty: Physics
Division: Solid State Physics
Group: Physics of surfaces and interfaces

Quantification in Low-Energy Ion Scattering

ROBERT J.M. ELFRINK FEBRUARI 1994

Master thesis

Mentors:

ir. J.-P. Jacobs
prof. dr. H.H. Brongersma

Voorwoord

Voor u ligt het verslag van mijn afstudeerproject, verricht in de groep 'fysica van oppervlakken en grenslagen' in de periode van januari 1993 tot februari 1994. Het vormt de afsluiting van mijn studie Technische Natuurkunde aan de Technische Universiteit Eindhoven.

Dit werk is tot stand gekomen dankzij de hulp van velen. Voor hun continue ondersteuning wil ik een aantal mensen hier bedanken.

Allereerst natuurlijke Jean-Paul voor zijn stimulerende begeleiding. Hij was altijd bereid om problemen op te lossen of resultaten te bespreken.
Daarnaast Hidde Brongersma voor de vele goede suggesties tijdens de discussies over de meetresultaten.
I also want to thank prof. dr. P.J. Scanlon from Queen's University, Kingston, Ontario, Canada. His experience and help have been of great value for the results presented in this work.
Sergei Mikhailov en Leon van den Oetelaar voor hun bijdrage aan de discussies.
Vacuum-expert Gerard Weyers en systeembeheerder Wijnand Dijkstra voor hun hulp bij technische storingen.
Kamergenoten Maarten, Stef, Martin, Hans (ook voor de discussies tijdens het 'apparaat onderzoek'), Hans, Serge en Roel en alle andere medeafstudeerders voor de ontspannen sfeer.
Verder al mijn vrienden, met name Jeroen en Mark, die ook de tijd buiten de studie tot een onvergetelijke maakten.
En als laatste, maar zeker niet in het minst, mijn ouders en broer voor hun continue steun tijdens mijn studie.

Robert.

Summary

Low-Energy Ion Scattering is a technique that can be used to perform surface analysis of the topmost atomic layer of a solid. Quantification of the surface composition was considered to be straightforward using calibration samples. Recently, it was shown that the ion signal intensities are not always independent of the chemical environment of an atom. In this work, the effect of target atom and chemical environment on the LEIS-intensity is studied.

In order to obtain a better understanding of the effect of different properties of the target on the neutralization of the incident noble gas ions, a number of pure metals have been measured at different primary energies. It was found that the neutralization is more important for elements for which ionization plays an important role. A qualitative explanation is given for this observation [38].

Quantification is possible in many practical cases, for example in alloys, by using calibration samples. However, this calibration method is only justified if the neutralization of the incident ions is independent on the chemical environment of the target atom (no matrix effects). The surface composition of three alloys, $Ni_{80}Pt_{20}$, NiAl(110) and $Ag_{80}Al_{20}$, has been determined using the calibration against pure elements. No matrix effects were observed for the NiPt and the AgAl alloy, but in NiAl(110) the neutralization for the Al was found to be different in the pure Al sample than in the alloy [50].

Contents

Chapter 1

Introduction

1.1 Surface physics

Surface science has been a subject of growing interest in the past decades. Scientists are aware of the major role of the outermost atomic layers of a solid in all kind of interesting phenomena, such as developments in the electronic industry, corrosion and catalysis.

Due to the high reactivity for gasses, it is necessary to study solid surfaces in ultra high vacuum (UHV). The interest in surface science has increased enormously since the development of UHV-equipment in the early sixties. A whole variety of surface science techniques has been developed and improved. Some of these techniques are listed in table 1.1.

In this work, the surface analysis technique Low-Energy Ion Scattering (LEIS) is used to study pure metals and alloys. An important advantage of Low-Energy Ion Scattering for surface analysis is that the information depth is limited to the outermost atomic layer.

1.2 Low-Energy Ion Scattering

In LEIS, the surface is probed by a mono-energetic beam of low-energy (keV) ions. Since the energy loss of the scattered ions depends on the mass of the target atom, the atomic composition of the target can be derived from the energy distribution of the scattered ions. When noble gas ions are used, the high neutralization probability ensures the monolayer sensitivity.

To quantify the composition, calibration against pure elements is used. However, this straightforward quantification presumes that the scattered ion intensities are independent on the chemical environment of an atom (no matrix effects). Recently, matrix effects in LEIS have been reported for some targets. For performing quantitative analysis, it is necessary to obtain a better understanding of the effect of projectile, target atom and chemical environment on the absolute LEIS signal.

One aim of this work is thus to study the effect of different properties of the target on the LEIS-signal by performing LEIS measurements on a number of pure metals and

electron spectroscopy		
	Auger Electron Spectroscopy	(AES)
	Ultraviolet Photo-electron Spectroscopy	(UPS)
	X-ray Photo-electron Spectroscopy	(XPS)
electron diffraction		
	Low-Energy Electron Diffraction	(LEED)
electron microscopy		
	Scanning Electron Microscopy	(SEM)
	Transmission Electron Microscopy	(TEM)
scanning probe microscopy		
	Scanning Tunneling Microscopy	(STM)
	Atomic Force Microscopy	(AFM)
photon spectroscopy		
	Infrared Spectroscopy	(IR)
	Raman Spectroscopy	
	Nuclear Magnetic Resonance	(NMR)
	X-ray Diffraction	(XRD)
ion scattering		
	Secondary Ion Mass Spectrometry	(SIMS)
	Low-Energy Ion Scattering	(LEIS, ISS)

Table 1.1: A selected list of surface analysis techniques.

semiconductors. Furthermore, attention is paid to the shape of the spectra, the energy position and width of the surface-peaks [38].

At present, the status of the theory and the restricted number of experimental data do not allow the prediction of the presence or absence of matrix effects in LEIS. Consequently, an other aim of this work is to study the effect of the chemical environment on the LEIS signal by quantitatively determining the surface composition of some alloys using the calibration against pure elements [50].

In chapter two, the theoretical aspects of LEIS are presented. In this work He^+ and Ne^+ incident ions are used with primary energies in the range of 1.0–3.5 keV. The scattering angle is 136°. All plots shown in this chapter are based on these parameters. In chapter three the experimental aspects are described. In chapter four the results on the pure elements are discussed and a model is presented to explain the results. In the next chapter the results on the alloys are shown. In the final chapter the conclusions are given, together with suggestions for future research.

Chapter 2

Low-Energy Ion Scattering: Theoretical aspects

2.1 Basic principles of LEIS

In Low-Energy Ion Scattering (LEIS), noble gas ions with energies in the range of 0.1–10 keV are directed onto the target. When an ion strikes the surface, it can pass the first atomic layer and penetrate the bulk, or it can be backscattered as ion or neutral. In LEIS only scattered *ions*, mainly resulting from collisions with atoms in the outermost atomic layer of the solid, are detected. Some typical physical parameters concerning the scattering process are listed in table 2.1 for 1 keV He^+-scattering from a Ni surface.

It can be seen from table 2.1 that diffraction effects are not relevant in LEIS since the De Broglie wavelength is much smaller than the lattice parameter. Furthermore, as a first approximation, the scattering process can be considered as a two body collision between the projectile and the individual target atom since the distance of closest approach is much smaller than the lattice parameter. The ion interacts with thermally displaced atoms at

		He^+	Solid (Ni)
Energy (eV)	Ionization potential	24.5	Workf. 5
Velocity (cm s^{-1})		$2*10^7$	$3*10^4$
Length (Å)	wavelength (λ) De Broglie closest approach	10^{-2} 0.2	Lattice par. 2–3
Time (s)	Collision time	$5*10^{-16}$	Vibrational period 10^{-13}

Table 2.1: Physical parameters relevant in LEIS (1 keV He^+ on Ni).

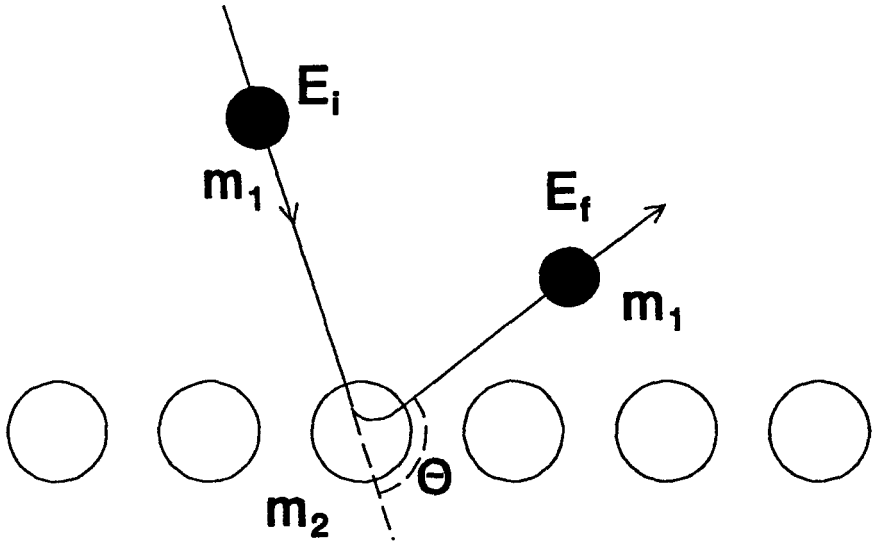

Figure 2.1: Schematic representation of the scattering process.

rest because thermal motions of the target atoms are slow compared to the ion interaction time.

In the LEIS-regime, the scattering process, schematically shown in figure 2.1, can be described using classical mechanics. Energy and momentum conservation gives that the final energy (E_f) of an ion only depends on the primary energy of the ion (E_i), the masses of ion (M_1) and target atom (M_2) and the scattering angle (Θ):

$$\frac{E_f}{E_i} = \left(\frac{\cos\Theta + \sqrt{A^2 - \sin^2\Theta}}{1 + A} \right)^2 \tag{2.1}$$

where

$$A = \frac{M_2}{M_1} > 1$$

When He^+ or Ne^+ are used as incident ions, the final energy of the scattered ions as function of the target mass is shown in figure 2.2. The final energy of the ions increases with the mass of the target atom, which means that an energy spectrum of the scattered ions is equivalent to a mass spectrum of the atoms at the surface. Figure 2.2 also shows that the mass resolution in the energy spectra is highest if the difference in mass between incident ion and target atom is small.

In general, there are three contributions to a LEIS-spectrum (see figure 2.3): the "surface peak", which is due to ions that had a collision with one single atom; a "reionization tail" at the low-energy side of the surface peak. This tail is due to ions that are first neutralized, penetrated deeper layers, scattered back towards the surface and reionized at a surface atom. At the high energy side of the binary collision peak, a tail is observed which is the result of ions that interacted with two or more atoms before scattering into

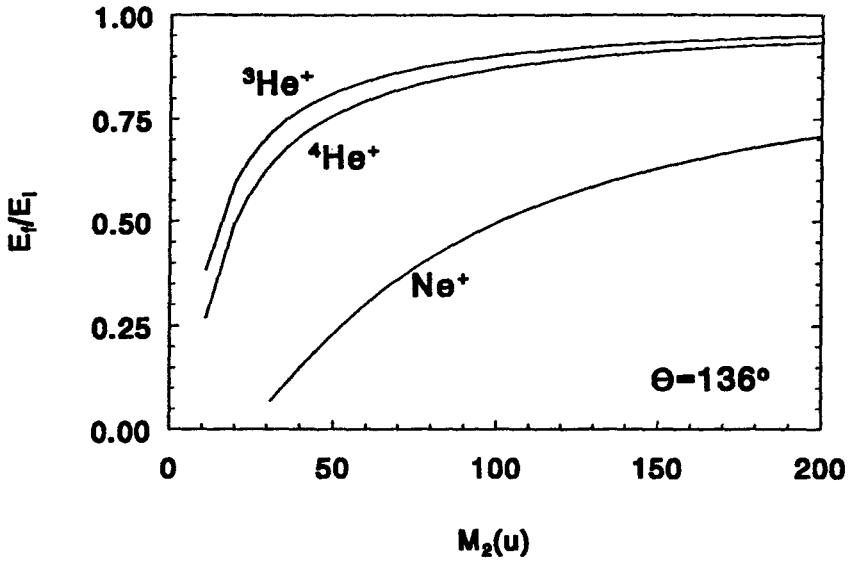

Figure 2.2: Ratio of final and primary energy for $^3He^+$, $^4He^+$ and $^{20}Ne^+$ incidence, as function of the mass of the target atom.

the analyzer. The shape of a LEIS spectrum will be discussed in more detail in chapter four.

2.2 Quantification in LEIS

The intensity of the surface peak for ions scattered from element i (S_i) can generally be expressed as [6]:

$$S_i = c' I_0 n_i \frac{d\sigma_i}{d\Omega} \Delta\Omega P_i^+ T = c I_0 n_i \frac{d\sigma_i}{d\Omega} P_i^+ E_f \tag{2.2}$$

where

I_0	= incident ion flux
n_i	= number of atoms of element i per surface area
$d\sigma_i/d\Omega$	= differential cross section for scattering of a particle by an isolated atom of element i into the analyzer
$\Delta\Omega$	= acceptance solid angle of the analyzer
T	= transmission of the analyzer ($\sim E_f$)
P_i^+	= ion fraction of backscattered particles
c', c	= proportionality factor depending on the analyzer and the detection efficiency

For quantification of the surface composition, n_i has to be determined. A direct quantification is only possible if the other parameters are known. In the next few paragraphs,

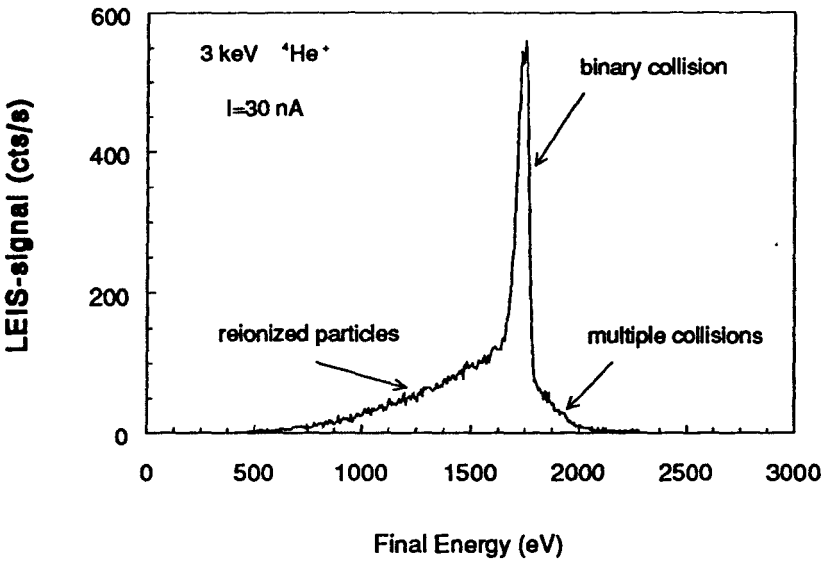

Figure 2.3: Typical LEIS spectrum: an Al-surface.

the effect of density of atoms at the surface, cross section, transmission behavior of the analyzer and ion fraction on the LEIS intensity will be discussed.

2.2.1 Surface density

The LEIS signal is proportional to the number of atoms of element i per surface area (see equation 2.2). The density of atoms at the surface for polycrystalline samples used in this work is listed in table 2.2.

As one can see from this table, the LEIS signal from different elements will not differ more than a factor of approximately 1.4 if only the density of atoms at the surface is taken into account. It will be shown in the next paragraphs that the effect of density on the LEIS-signal from different elements is small compared to the effect of cross section and ion fraction.

element	n $*10^{15}cm^{-2}$	element	n $*10^{15}cm^{-2}$	element	n $*10^{15}cm^{-2}$
Cu	1.93	Cr	1.93	Rh	1.74
Ni	2.04	Mo	1.62	Ir	1.70
Pd	1.66	W	1.58	Al	1.55
Pt	1.62	Ta	1.46	Si	1.70

Table 2.2: Density of atoms at the surface of polycrystalline elements studied in this work.

2.2.2 Differential cross section

The differential cross section for a given direction is defined as the fraction of the incident intensity scattered into unit solid angle about this direction. The cross section can be calculated using classical collision theory, provided that the interaction between ion and atom is known. This interaction is described by an interatomic potential. In the keV energy range, the repulsive interaction between an ion and an atom is determined by their nuclear charge and the screening of this charge by the electron clouds. Therefore, screened Coulomb potentials are usually considered that have the general form [1]:

$$V(r) = \frac{Z_1 Z_2 e^2}{4\pi\epsilon_0 r}\phi(\frac{r}{a}) \tag{2.3}$$

where $\phi(\frac{r}{a})$ is called the screening function and a the screening length.

Nowadays, the Molière approximation to the Thomas-Fermi screening function is widely used. In this approximation, $\phi(\frac{r}{a})$ is written as [3]:

$$\phi(\frac{r}{a}) = 0.35\exp\left(-0.3\frac{r}{a}\right) + 0.55\exp\left(-1.2\frac{r}{a}\right) + 0.10\exp\left(-6\frac{r}{a}\right) \tag{2.4}$$

and

$$a = \frac{0.88534\, a_0}{\left(\sqrt{Z_1} + \sqrt{Z_2}\right)^{\frac{2}{3}}} \tag{2.5}$$

where a_0 is the Bohr atomic radius.

To illustrate the effect of screening of the nuclear charge by the electron clouds, both Coulomb and Molière potential are presented for He and Ne ions interacting with Si and W in figure 2.4. The interaction range of the Molière potential is restricted to approximately 1 Å. Only at very small distances ($r/a << 1$) the Molière potential is equivalent to the Coulomb potential ($\phi \rightarrow 1$).

Using the Molière potential, the relevant parameters for the scattering process, such as the impact parameter b, the distance of closest approach s_0 and the differential cross section (see figure 2.5) can be calculated. Values for these parameters are shown in figure 2.6 at 1 and 3.5 keV incident He^+ and Ne^+, as function of the mass of the target atom.

All parameters increase monotonously with increasing mass of the target atom and decrease with increasing primary energy. Typical distances of closest approach are 0.2 Å for He^+ scattering and 0.4 Å for Ne^+ scattering. Due to the cross section only, the LEIS signal increases approximately one order of magnitude when going from light to heavy elements. The effect of different primary energies (1 and 3.5 keV) on the LEIS signal due to the cross section only, is approximately a factor of 3.

2.2.3 Transmission of the analyzer

The ions are energy analyzed using a modified Cylindrical Mirror Analyzer (CMA). The detection will be described in more detail in the experimental chapter. An important

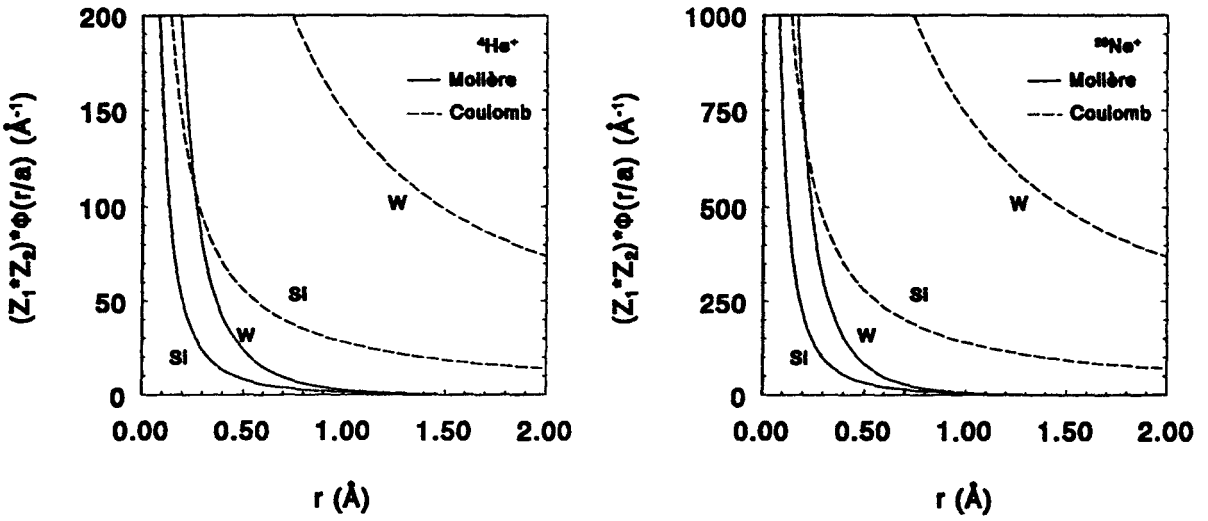

Figure 2.4: Comparison of Molière potential and Coulomb potential for He and Ne ions interacting with Si and W.

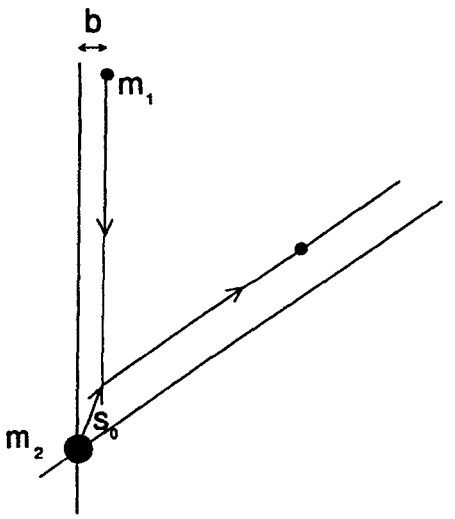

Figure 2.5: Two parameters that determine the scattering process: the impact parameter b and the distance of closest approach s_0.

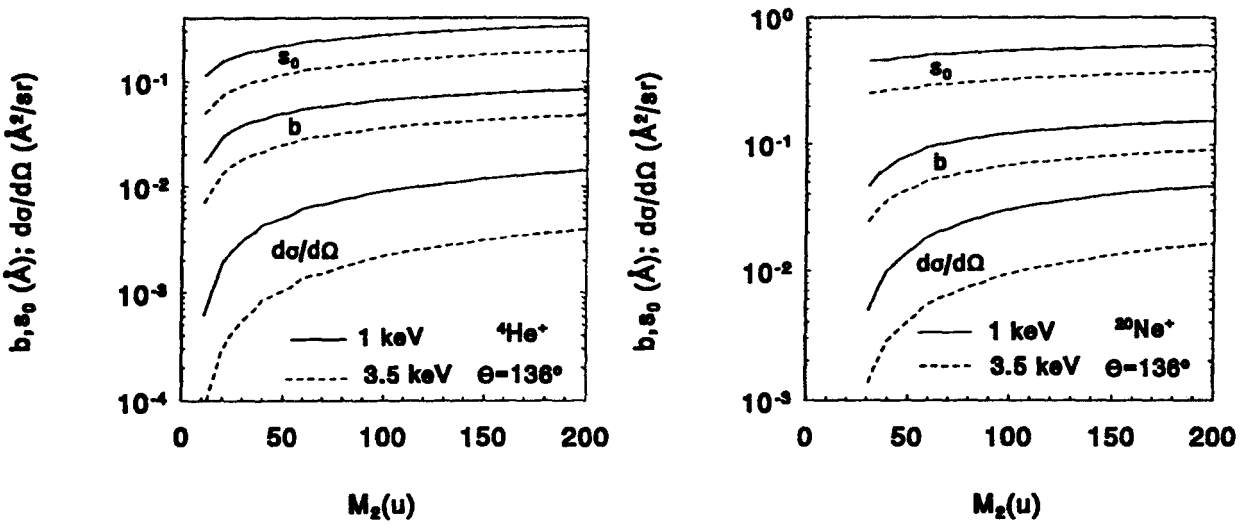

Figure 2.6: The impact parameter b, the distance of closest approach s_0 and the differential cross section $d\sigma/d\Omega$, calculated using the Molière potential.

property of the CMA is the fact that $\Delta E/E$ is constant [4]. This implies that the width of the surface peak and thus the LEIS signal is proportional to the final energy of the scattered ions.

The effect of both cross section and final energy (calculated using equation 2.1) on the LEIS signal as function of the mass of the target atom is shown in figure 2.7.

Comparing this to figure 2.6, where only the cross section was taken into account, we can conclude that both cross section and transmission behavior of the analyzer give rise to an increase in the LEIS signal of approximately two orders of magnitude when going from light to heavy target elements. Furthermore the effect of the primary energy is much smaller now.

2.2.4 Ion fraction

The cross section reflects the probability that a particle is scattered into a certain direction, independent of the charge state of this particle. Since in LEIS only scattered *ions* contribute to the signal, the cross section has to be multiplied by an ion fraction. The ion fraction is defined as the number of ions divided by the total number of particles (ions plus neutrals) scattered in a certain direction, $I/(I+N)$.

The ion fraction is determined by the charge exchange processes neutralization and ionization. Neutralization of primary ions is a very important phenomenon in LEIS, since high neutralization probabilities make LEIS extremely surface sensitive.

However, neutralization and thus the ion fraction, is strongly dependent on ion-atom combination, incident energy of the ions and the scattering angle. The lack of understanding the ion fraction behavior is the most important reason why direct quantification in

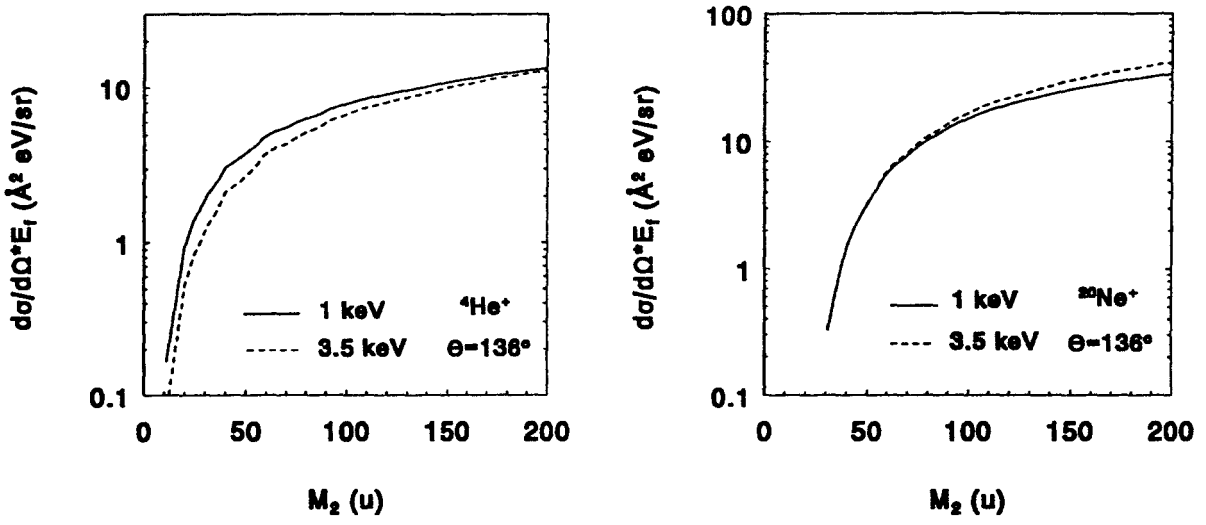

Figure 2.7: Effect of cross section and transmission behavior of the analyzer on the LEIS signal as function of target mass. No influence of density of atoms at the surface is taken into account. Furthermore, the ion fraction is assumed 1 for all masses.

LEIS is still impossible.

The charge state of the particle after scattering, and thus the behavior of the ion fraction, is determined by the charge exchange processes, neutralization and ionization. Before deriving a quantitative expression for the ion fraction, the various neutralization processes will be discussed.

Neutralization processes

The basic mechanisms for neutralization, first described by Hagstrum [5], are Auger neutralization, valence level resonance neutralization, core level resonance neutralization and radiative neutralization (see figure 2.8).

In radiative neutralization, an electron is transferred from the surface valence band to the 1s level of the He-ion. The energy is used to emit a photon. The probability for radiative neutralization is very low because the lifetime for radiation ($\approx 10^{-8}$ s) is very long compared to the time an ion spends within a few angstroms units of the surface ($\approx 10^{-16}$ s).

When the ground state of the ion is close to a core level of a target atom, core level resonance neutralization is possible. For He^+ scattering this process is observed for a number of target atoms (In, Pb, Ge, Bi, Sn) [6]. In general, Auger neutralization and valence level resonance neutralization are thought to be the dominating processes.

In Auger neutralization an electron is transferred from the surface valence band to the 1s level of the ion. The energy is used to emit an other electron. This process can occur if the ion approaches a particular surface atom at a distance as small as 2 Å, so that the

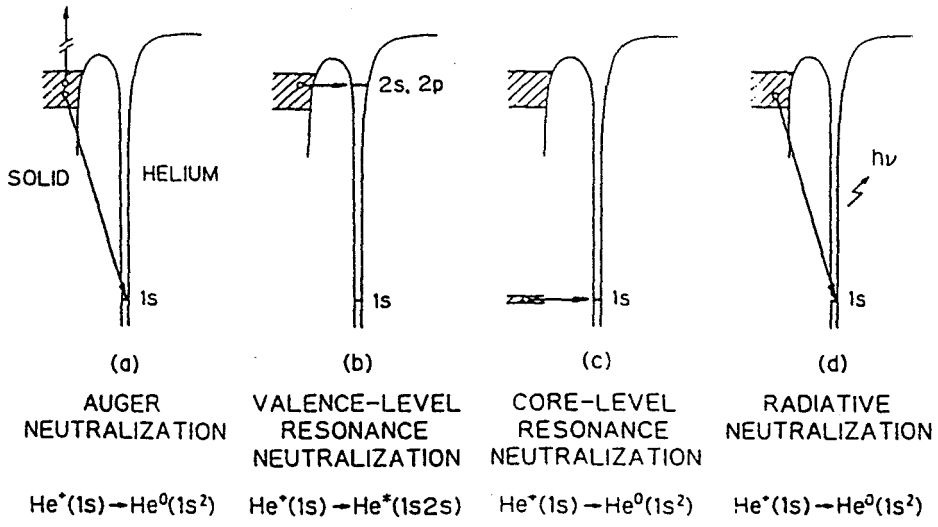

Figure 2.8: Possible mechanisms of neutralization of noble gas ions at solid surfaces [7]

He 1s orbital appreciably overlaps the valence electron cloud of the surface atom.

In valence level resonance neutralization an electron is transferred from the surface valence band to the 2s-or 2p level of the ion. This process can occur at larger distances from the surface (<5 Å), since an overlap between the 2s orbital of the ion and the valence electron cloud of the atom is required. The probability for this process strongly depends on the workfunction of the target material; Souda et al. [7, 8] showed that for surfaces with workfunctions as large as about 4 eV valence level resonance neutralization is almost impossible since the reverse process ($He^* \rightarrow He^+$, resonance ionization of an excited atom) was found to occur with a probability close to unity. They conclude therefore that Auger neutralization is the dominating process, provided the workfunction is larger than 4 eV. For smaller workfunctions also valence level resonance neutralization may become important.

Hagstrum model for metal surfaces

The physical model describing Auger neutralization of ions close to a surface was first developed by Hagstrum [5]. Although this model was derived for ions with energies up to a few hundred eV, it is often used for the LEIS-regime (keV). Since only metallic surfaces were studied, the electron density at the surface was considered homogeneous. The basic concept of this model is a transition rate for Auger neutralization that exponentially depends on the distance s between ion and surface:

$$R(s) = A \exp(-a\, s) \tag{2.6}$$

where A is a pre-exponential constant and a determines the ion-surface interaction range.

Using this equation, the probability for Auger neutralization on the inward trip of the

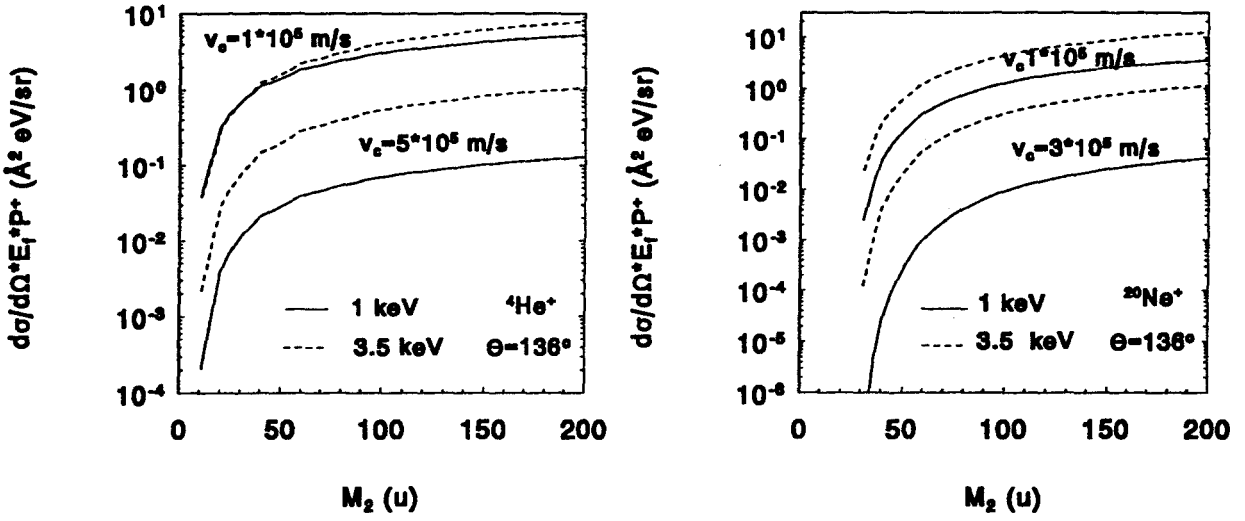

Figure 2.9: Effect of cross section, transmission behavior of the analyzer and ion fraction on the LEIS signal for different v_c-values as function of mass of the target atom. No influence of density of atoms at the surface is taken into account.

ion towards the metal surface can be calculated [5]:

$$P_{neutr} = 1 - \exp(-\frac{A}{av_i}) \tag{2.7}$$

The probability of an ion to survive neutralization both on the inward and the outward trip away from the metal can thus be written as:

$$P^+ = \exp\left(-\frac{A}{a}\left(\frac{1}{v_i} + \frac{1}{v_f}\right)\right) = \exp\left(-v_c\left(\frac{1}{v_i} + \frac{1}{v_f}\right)\right) \tag{2.8}$$

where v_i and v_f are the velocities resp. before and after the collision and v_c is a neutralization constant, often called characteristic velocity, which strongly depends on the ion-target combination.

Equation 2.8 can be interpreted as a neutralization probability which exponentially depends on the time the ion spends within a certain distance from the surface. In chapter 4 it will be shown that values for v_c are of the order of a few times 10^5 m/s for He^+ scattering from metal surfaces. The effect of the characteristic velocity on the absolute LEIS signal is shown in figure 2.9 for different primary energies. The final velocity of the ion was calculated using the binary collision model.

The effect of v_c on the LEIS signal is enormous, especially at low primary energies. For the same target mass, a difference of about 50-100 is found at 1 keV He^+ when using v_c-values of $1*10^5$ m/s and $5*10^5$ m/s. Furthermore, due to the total of cross section, transmission behavior of the analyzer and ion fraction, the LEIS-signal changes approximately three orders of magnitude for He^+ scattering from light and heavy target atoms at

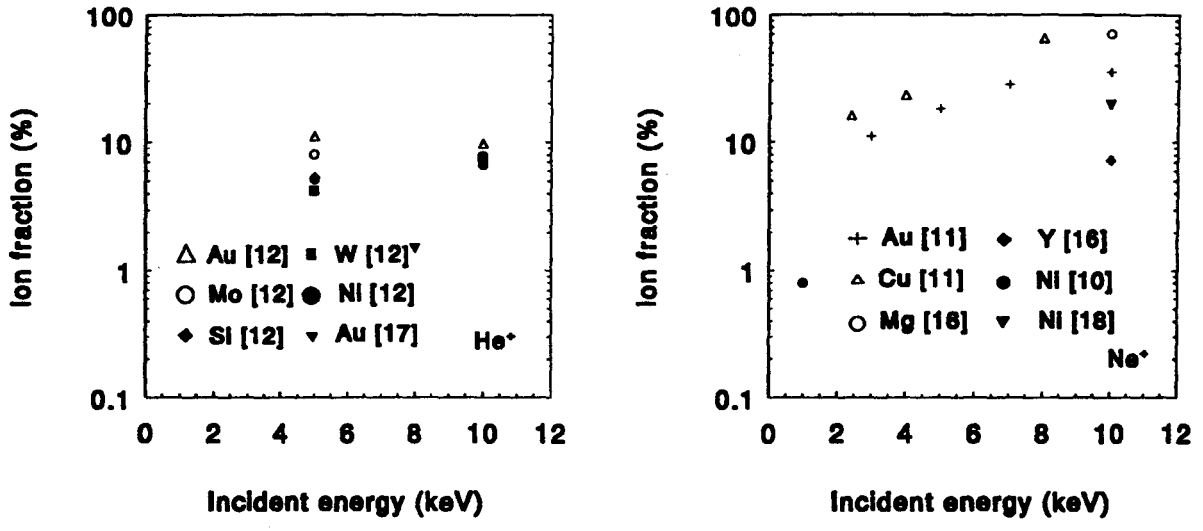

Figure 2.10: Absolute data on ion fractions, reported in literature.

a v_c-value of $5*10^5$ m/s. For direct quantification it is essential to have values for v_c for different elements. One of the most important parts of this work is thus to determine v_c for different elements and try to understand it's dependence on target atom.

Ion fractions in literature

A number of investigators, [6, 9, 10, 11], observed the behavior for the ion fraction as predicted by Hagstrum. However, some others found that the measured ion fraction did not show the predicted behavior [12]. Verhey et al. [13] and O'Connor et al. [14, 15] report characteristic velocities which are energy dependent. According to Rabalais et al. [16] equation 2.8 is only valid in a certain energy range, that depends on target and scattering angle.

Absolute data on ion fractions reported in literature were measured using the Time of Flight (TOF) technique, where both neutrals and ions are detected [11, 17] or by ionizing the neutrals [12]. In figure 2.10 absolute ion fractions reported in literature are summarized. The large spread in ion fractions for different energies and targets indicate the importance of this factor for quantification. In spite of the lower velocity and thus longer time for neutralization for Ne ions, the ion fractions are even higher than for He^+ scattering. A possible explanation for this is the autoionization process: an incident Ne ion is neutralized on the way to the surface. Atomic levels of the target and projectile atom merge into molecular orbitals (MO's). Electrons formerly in lower-energy atomic states are promoted into higher-energy MO's and, as the atoms separate, electrons in the projectile atom are left in excited atomic levels. These excited projectile atoms then decay by an Auger autoionizing process emitting energetic electrons. Due to the long lifetime of the excited state, the autoionization of the excited atoms occur relatively far from the surface where

1	H 1s																He $1s^2$
2	Li 2s ·	Be $2s^2$											B 2p $2s^2$	C $2p^2$ $2s^2$ ≤200	N $2p^3$ $2s^2$	O $2p^4$ $2s^2$	F $2p^5$ $2s^2$ —	Ne $2p^6$ $2s^2$
3	Na 3s ≤200	Mg $3s^2$ ≤200	ELEMENT ELECTRON CONFIGURATION THRESHOLD ENERGY FOR REIONIZATION (eV)										Al 3p $3s^2$ 300	Si $3p^2$ $3s^2$ 300	P $3p^3$ $3s^2$	S $3p^4$ $3s^2$	Cl $3p^5$ $3s^2$ —	Ar $3p^6$ $3s^2$
4	K 4s ≤200	Ca $4s^2$ ≤200	Sc 3d $4s^2$	Ti $3d^2$ $4s^2$ ≤200	V $3d^3$ $4s^2$	Cr $3d^4$ $4s^2$	Mn $3d^5$ $4s^2$ 500	Fe $3d^6$ $4s^2$	Co $3d^7$ $4s^2$ —	Ni $3d^8$ $4s^2$ —	Cu $3d^{10}$ $4s^2$ —	Zn $3d^{10}$ $4s^2$ —	Ga 4p $4s^2$	Ge $4p^2$ $4s^2$ —	As $4p^3$ $4s^2$	Se $4p^4$ $4s^2$	Br $4p^5$ $4s^2$	Kr $4p^6$ $4s^2$
5	Rb 5s	Sr $5s^2$ ≤200	Y 4d $5s^2$ 300	Zr $4d^2$ $5s^2$ 300	Nb $4d^4$ 5s	Mo $4d^5$ 5s 400	Tc $4d^6$ 5s	Ru $4d^7$ 5s	Rh $4d^8$ 5s	Pd $4d^{10}$ —	Ag $4d^{10}$ 5s —	Cd $4d^{10}$ $5s^2$ —	In 5p $5s^2$ —	Sn $5p^2$ $5s^2$ 600	Sb $5p^3$ $5s^2$ 1100	Te $5p^4$ $5s^2$ 1200	I $5p^5$ $5s^2$ —	Xe $5p^6$ $5s^2$
6	Cs 6s	Ba $6s^2$	La 5d $6s^2$	Hf $5d^2$ $6s^2$	Ta $5d^3$ $6s^2$ 300	W $5d^4$ $6s^2$	Re $5d^5$ $6s^2$	Os $5d^6$ $6s^2$	Ir $5d^9$ —	Pt $5d^9$ 6s	Au $5d^{10}$ 6s	Hg $5d^{10}$ $6s^2$	Tl 6p $6s^2$	Pb $6p^2$ $6s^2$ —	Bi $6p^3$ $6s^2$	Po $6p^4$ $6s^2$	At $6p^5$ $6s^2$	Rn $6p^6$ $6s^2$

Table 2.3: Threshold values of the primary He^+ energy for reionization measured for 29 target elements. — means larger than 2000 eV [7].

additional neutralization is unlikely [11].

2.3 Reionization

Another important charge exchange process in LEIS is ionization of neutralized projectiles. In LEIS spectra often a tail is observed at the low energy side of the surface peak (see figure 2.3). These lower energy ions originate from incident ions that were neutralized when penetrating the bulk, scattered back towards the surface and reionized at a surface atom. The energy loss depends on the length of the trajectory of the particle through the solid [19].

Souda et al. [7] found, by using a He^0 incident beam on 29 targets, that for reionization a minimum energy (threshold energy) is required. The threshold energy strongly depends on the target (see table 2.3). It can be seen from this table that the threshold energy increases in the fourth and fifth period as the number of d-electrons increases. A small threshold is observed for Sn, but as the number of 5p electrons increases, the threshold energy increases. The same tendency is found in the second and third period. Electron transfer to the target thus seems to be suppressed if the target atom does not have empty valence levels.

The mechanism of reionization proposed by Aono et al. [20] is schematically shown in figure 2.11, where curve I shows the total energy of the whole of He^0 and target atom M as function of the distance between He^0 and M and curve II shows a similar plot for He^+ and M^-. At small distances a quasimolecule 'HeM' is formed if the energy levels I and II cross.

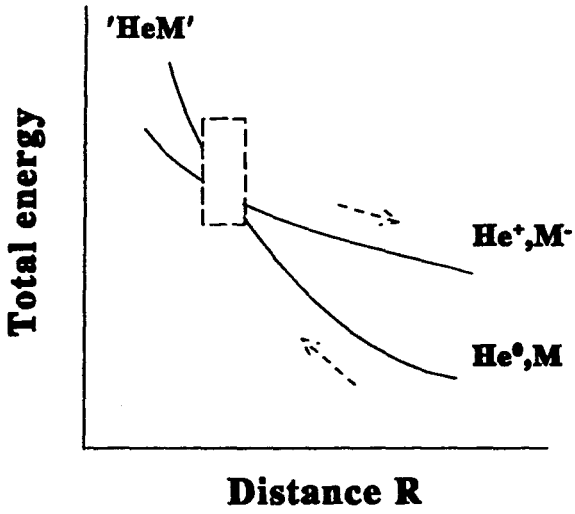

Figure 2.11: Schematic figure showing the mechanism of ionization of He^0 [7].

The He^0 can be ionized through the path $He^0 + M \rightarrow$ 'HeM' $\rightarrow He^+ + M^-$. Crossing of the levels occurs if there exists a strong antibonding interaction between the He 1s level and a core level of the target atom, which will raise the He 1s level with decreasing distance to the surface atom. For He-Ti interaction Aono et al. [20] have observed level crossing, whereas for the He-Cu combination no level crossing was found, which is consistent with the difference in threshold energy (table 2.3).

2.4 Summary

In this chapter, the effect of different parameters, such as density of atoms at the surface, transmission behavior of the analyzer, differential cross section and ion fraction, on the LEIS-intensity was discussed. The cross section only, gives rise to a change in absolute LEIS-signal of approximately one order of magnitude when going from light to heavy elements. If also the transmission behavior of the analyzer is taken into account, a change of two orders of magnitude on the LEIS-signal is found when going from light to heavy elements.

The charge state of the particle after scattering is determined by both neutralization (mainly Auger) and reionization. The ion fraction is defined as the ratio of number of ions and total number of particles (ions plus neutrals) scattered in a certain direction. According to a model proposed by Hagstrum, the ion fraction can quantitatively be expressed as $P^+ = \exp(-v_c(1/v_i + 1/v_f))$. The effect of the characteristic velocity on the absolute LEIS-signal is enormous. The values for v_c are unknown and will depend on the target. For direct quantification in LEIS, it is necessary to have values for v_c.

The probability for reionization strongly depends on the target atom, and is found to

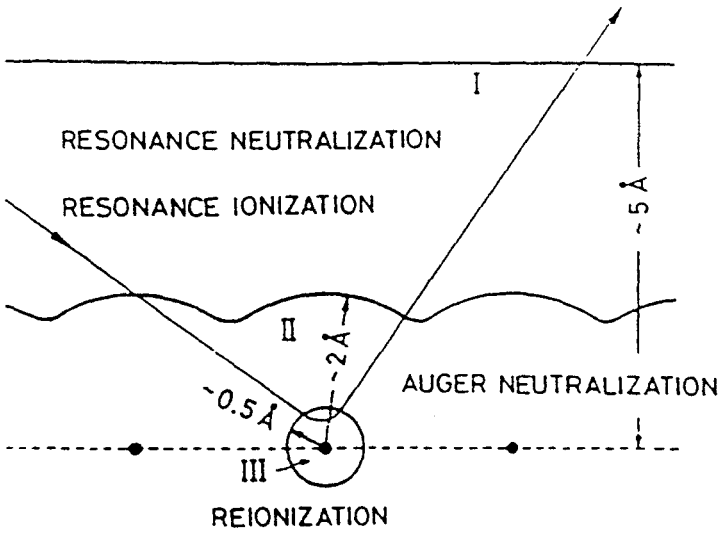

Figure 2.12: Three different spatial region, I, II and III where resonance neutralization, Auger neutralization and reionization occur, respectively [7].

decrease with increasing number of d-electrons. The reionization process can qualitatively be explained by a level crossing model.

The spatial region where the basic charge exchange processes in LEIS occur, are schematically shown in figure 2.12.

Chapter 3

Low-Energy Ion Scattering: Experimental aspects

3.1 Experimental setup, the Mini MOBIS

In our group several experimental techniques are available for studying different properties of a surface: Low-Energy Ion Scattering, Low-Energy Electron Diffraction, ellipsometry, Atomic Force Microscopy, Secondary Ion Mass Spectroscopy, Auger Electron Spectroscopy and X-ray Photoelectron Spectroscopy. All experiments done in this work have been performed on the LEIS apparatus Mini MOBIS, which stands for MOdular Backscattered Ion Spectrometer. The setup is schematically shown in figure 3.1. It is similar to the NODUS-machine, which basic design is described earlier [21].

3.1.1 Vacuum system

Since LEIS is very sensitive to the outermost atomic layer, contamination of the surface should be avoided as much as possible. Therefore, the measurements are performed in Ultra High Vacuum (UHV). The base pressure in the main chamber is in the low 10^{-10} mbar range by pumping the chamber with a turbo molecular pump, an ion getter pump and a titanium sublimation pump, which is cooled by liquid nitrogen. During experiments, the pressure increases to the low 10^{-9} mbar range due to the influx of inert gas, which doesn't effect the measurements. The composition of gasses in the chamber can be determined by a mass spectrometer.

The samples are positioned onto a carrousel, which can contain 10 samples at the same time. This allows to measure different samples under identical experimental conditions. The samples can be cleaned in situ by ion (mostly Ar^+) bombardment using the sputter ion source (angle of incidence 15°). Each sample can be heated by an oven to a temperature of approximately 750 °C. New samples can be inserted in the main chamber through a transfer-room, which is pumped by a turbo molecular pump. In this way, inserting a new sample can be done quite fast, while the vacuum in the main chamber is hardly affected. The transfer-room can also be used for pretreatments of a sample in, for example, oxygen

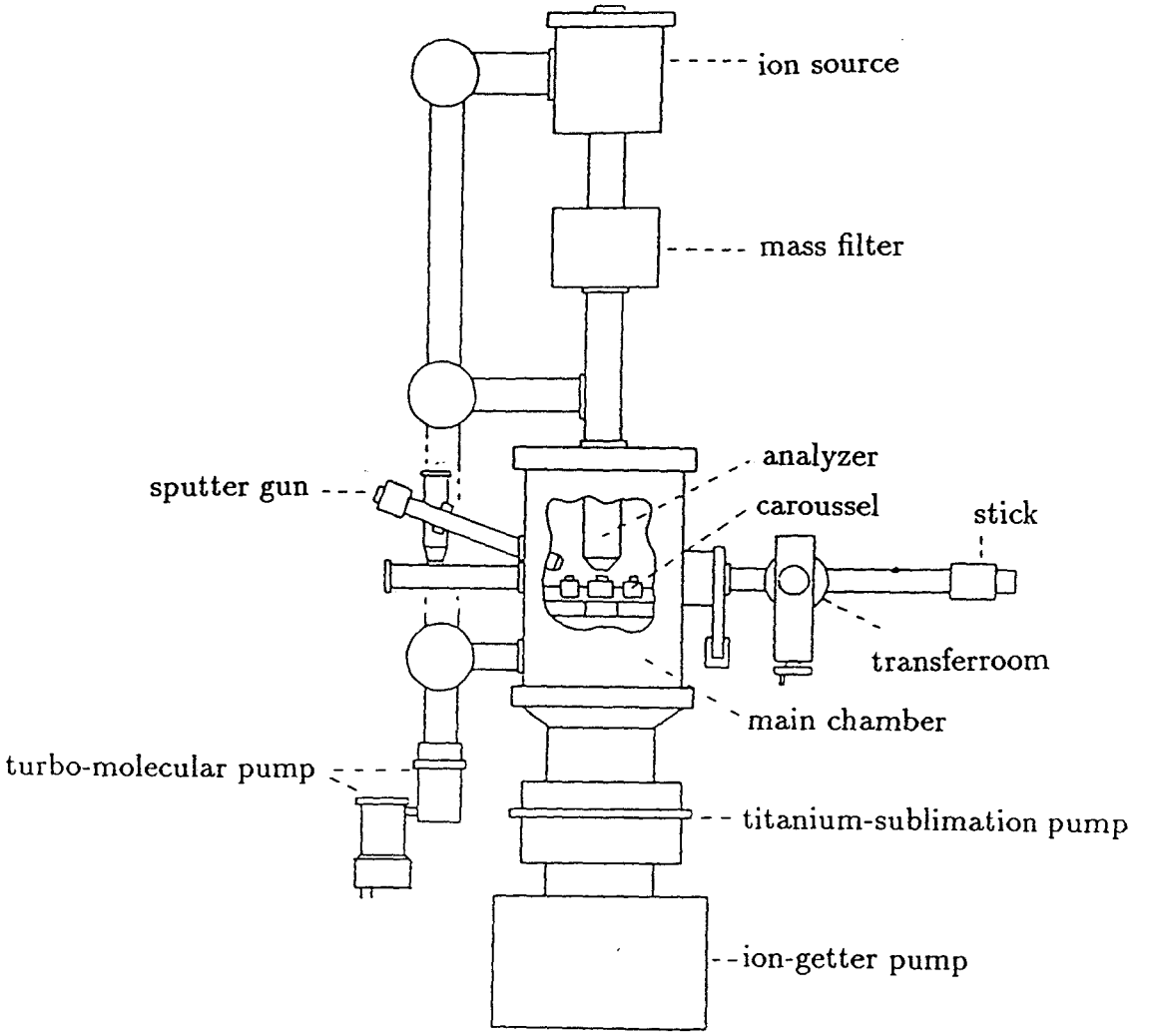

Figure 3.1: Schematical representation of the experimental setup, the Mini MOBIS.

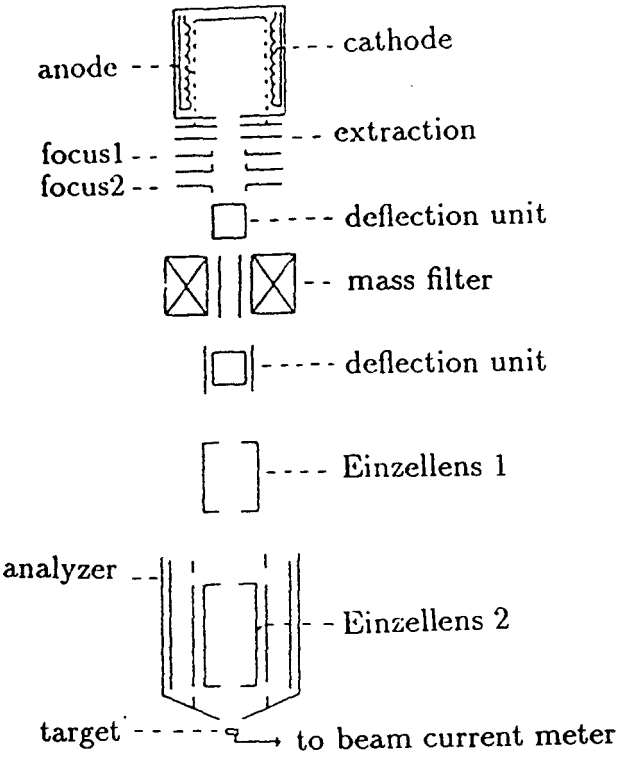

Figure 3.2: Trajectory of the ion beam.

or hydrogen ($10^{-6} < p < 10^{3}$ mbar). During this pretreatment, the sample can be heated up to approximately 400 °C.

3.1.2 Ion beam

The incident ion energy can be varied between 500 and 5000 eV. After extraction from the ion source, the ion beam passes a mass filter and several focusing and deflection units (see figure 3.2). As primary ions $^{4}He^{+}$, $^{3}He^{+}$, Ne^{+}, Ar^{+} or H^{+} can be used. The ion beam is directed perpendicularly onto the target. The minimum spot size at the target is approximately 1 mm^{2} but it's size can be varied by changing the focusing settings.

3.1.3 Analysis and detection

The ions scattered from the sample through an angle of 136 ° degrees are energy analyzed by a modified Cylindrical Mirror Analyzer (CMA) (see figure 3.3). The CMA is designed to give a ring-shaped focus around its geometric axis for ions with a specific energy. The energy of the ions that pass the CMA can be selected by varying the voltage of the outer cylinder of the CMA. After passing the CMA, the ions are detected by a set of eight channeltrons which cover the major part of the focus ring. To prevent (secondary) electrons from striking the channeltrons, the ions are postaccelerated (-100 V). The ions impinging

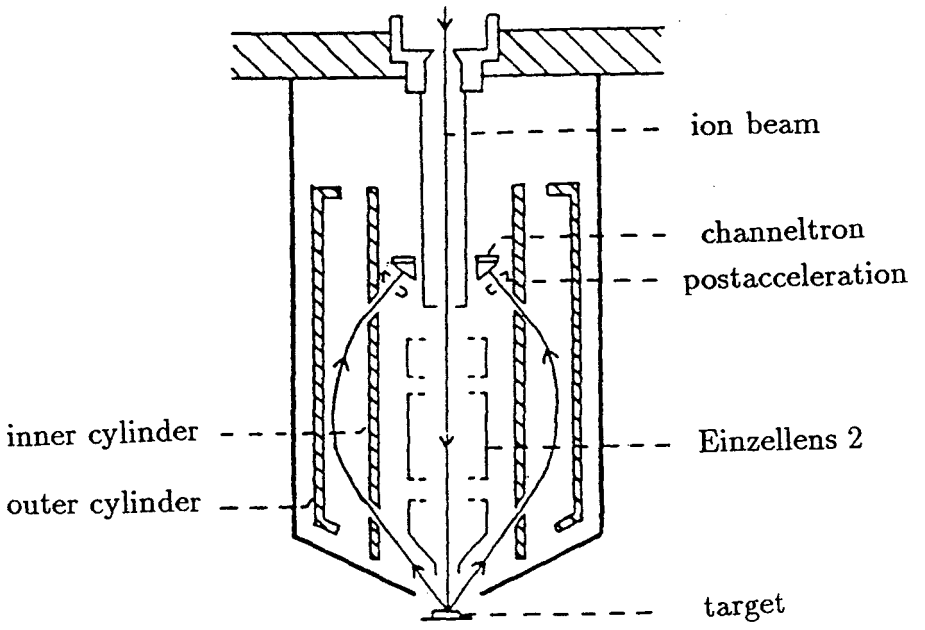

Figure 3.3: Schematic view of the electrostatic analyzer (CMA) of the Mini MOBIS.

on a channeltron generate secondary electrons, which induce a electron cascade. If the multiplied current pulse (V) (after amplification) exceeds the discriminator level, the pulse is counted. During this work the discriminator level (2.1 V) was found to be far above the noise level ($\approx$ 0.4 V). As a consequence of this, only a small part of the ions striking the channeltrons was counted. Moreover, the counted fraction strongly depended on the energy of the ions, because the channeltrons were not in the saturated mode. All results had to be corrected for this. A more detailed description of this correction can be found in appendix A.

3.2 Experimental procedure

3.2.1 Sample cleaning

In this work the following samples have been studied: Cu, Al, Cr (polycrystalline samples), Rh, Ta, Ir, Pd, Pt, Mo, W (polycrystalline ribbons), Ni(100), Si(100) (single crystals) and the alloys, NiAl(100) [42], $Ag_{80}Al_{20}$ and $Ni_{80}Pt_{20}$. The targets were cleaned by repeated cycles of sputtering by 5 keV Ar^+ ions (for single crystal lower energies were used) and heating of the sample. The maximum temperature that can be reached with the oven is approximately 750 °C. The ribbons could be heated to much higher temperatures using resistive heating. To remove carbon from the surface, some samples were heated in a 10^{-7} mbar oxygen atmosphere prior to the measurements.

3.2.2 Measuring procedure

To ensure identical conditions, the ion beam is always calibrated using a Cu polycrystalline reference target. The pure metals have been measured using 1.0, 1.5, 2.0, 2.5, 3.0 and 3.5 keV incident $^3He^+$, $^4He^+$ or $^{20}Ne^+$ ions. The beam current at the target was kept constant at all energies ($\approx$ 30 nA) by varying the gas pressure in the ion source.

The total current at the target consists of primary ions, scattered ions and secondary electrons. The scattered ion current is assumed small because of the high neutralization probability for the inert gas ions. To prevent secondary electrons from contributing to the current, the primary ion current is measured when the sample is at a positive voltage (34 V).

The target position is optimized on maximum backscattered ion signal. The LEIS signal is determined by integrating the surface peak area after linear background subtraction.

3.3 Surface damage

Due to the bombardment of the sample by the primary ion beam, the sample will be damaged. The sputtering effect of the ion beam can be used to obtain compositional depth profiles of near surface layers. However, often one is only interested in the outermost atomic layer. The damage to the surface should then be minimized because the surface structure may change on a macroscopic scale.

The number of sputtered particles (N) per unit surface area can be expressed as:

$$N = \frac{I\,t\,Y}{e\,A} \tag{3.1}$$

where

- I : incident ion current
- t : measuring time
- Y : sputteryield
- e : unit charge
- A : beam spot size at the target

In this work incident currents of 30 nA are used. The spot size is estimated to be 1 mm^2. Assuming a sputteryield of 10 % for He ions on metal surfaces, the number of sputtered particles per measured spectrum ($\approx$100 s) is $1.9*10^{14}$ cm^{-2}. This means that 1 monolayer is removed during the recording of 5 spectra, since in general the density of atoms at the surface is of the order of 10^{15} cm^{-2}.

Chapter 4

Low-Energy Ion Scattering from Metals

4.1 Introduction

In this chapter, the results for He^+-scattering from pure metals are presented. First, attention is paid to the shape of the LEIS-spectra, i.e. the reionization tail, the energy-position and width of the surface peak. Next, the neutralization constants are determined for each element. The effect of different properties of the target on neutralization will be discussed and a qualitative model is presented to explain the results.

4.2 Shape of LEIS spectra

The measured spectra on pure metals using 1.0–3.5 keV $^4He^+$ and $^{20}Ne^+$ are shown in appendix B. The shape of the spectra will be discussed here. In figure 4.1 some parameters determining the shape of a spectrum are schematically shown.

4.2.1 Reionization tails

Results

As discussed in chapter 2, an ion which is neutralized can be reionized during the interaction with a surface atom. As a result of this process, often a tail at the low-energy side of the surface peak is observed. For the elements studied, two values are listed in table 4.1 to characterize the reionization behavior of an element (see also figure 4.1):

- threshold energy E_{thr} (low-energy edge of tail)
- tail to peak height (TP) ratio for 3 keV $^4He^+$

It follows from this table that, as was pointed out by Aono et al. [20], elements with filled d bands (such as Cu, Ni, Pd) hardly reionize neutrals, while elements with empty d bands

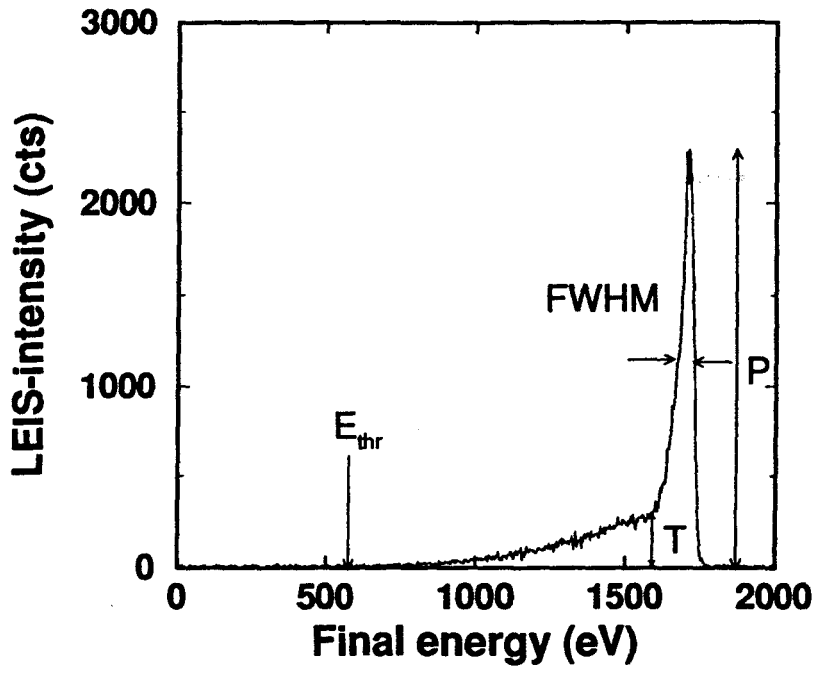

Figure 4.1: Definitions of parameters determining the shape of a LEIS spectrum: low-energy edge of the tail as threshold energy for reionization (E_{thr}), Full Width Half Maximum (FWHM) of the surface peak and height of tail (T) and peak (P).

element	E_{thr} (eV)	TP-ratio	element	E_{thr} (eV)	TP-ratio
Cu	1650	0.01	Al	400	0.22
Ni	1400	0.01	Si	400	0.10
Pd	1150	0.05	Mo	500	0.25
Pt	1250	0.03	Cr	500	0.19
Rh	850	0.12	Ta	350	0.15
Ir	850	0.17	W	450	0.30

Table 4.1: Threshold energies for reionization and tail to peak height (TP)-ratios for He^+-scattering from the elements studied in this work.

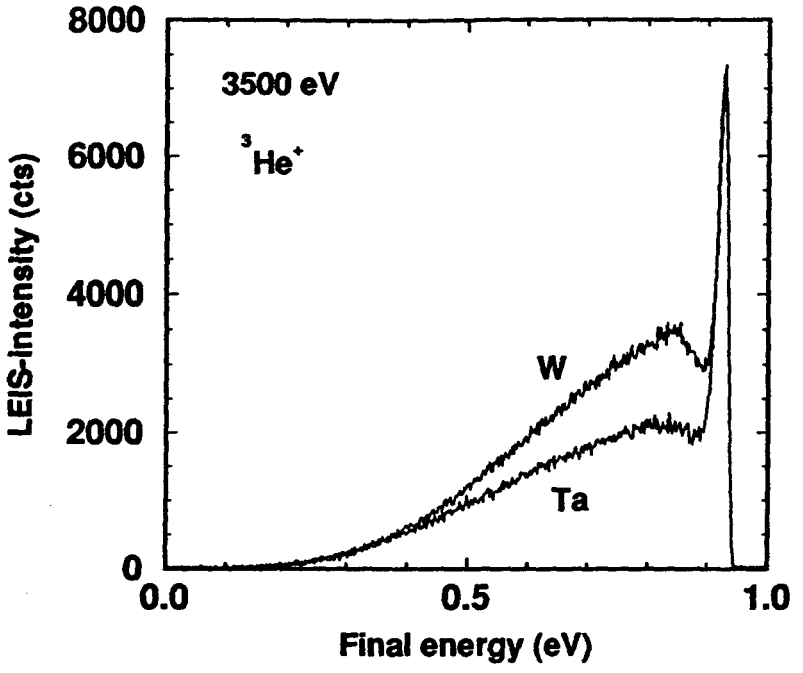

Figure 4.2: LEIS-spectrum of 3.5 keV $^3He^+$ incident on Ta and W.

(such as W, Ta, Cr, Mo) easily reionize. The measured threshold energies agree reasonably well with the values reported by Aono et al. [7] (see also table 2.3).

In the high energy spectra of W and, to lesser extend Ta, a maximum in the tail is observed at an energy position of approximately E_f/E_i=0.84 (see figure 4.2). For W this was also found by Pierson et al. [22].

The maximum in the tail seems similar to a peak observed by Thomas et al. [23]. They scattered both He^+ (ISS) and He^0 (NSS) from 16 elements and found two peaks in the NSS-spectra, I_S and I_B. I_S (see figure 4.3) was attributed to scattering from the surface monolayer, whereas I_B was attributed to sub-surface scattering. The intensity of the sub-surface peak was found to be strongly dependent on the element and the I_B/I_S ratio was highest for C, Cr, Mo, Ta and W. The ratio of the NSS-signal and the ISS-signal was also determined for different primary energies and is summarized in table 4.2 for the elements which are of interest in this work.

As can be seen from this table, the NSS-signal is only a few percent of the ISS-signal. The ratio NSS/ISS is highest for Ta and W and it rapidly increases with energy. Since the energy position of the maximum in the tail for Ta corresponds to the energy position of the I_B-peak in the NSS spectra of Thomas et al., this might be attributed to the same sub-surface scattering.

The maximum is thus probably the result of ions that are first neutralized, scattered from sub-surface atoms and reionized. Probably this peak also exists for the other elements, but its intensity is too low to be detected (see table 4.2). W and Ta have both low threshold energies for reionization and high mass which means a high final energy of the ions and thus a higher probability to survive neutralization.

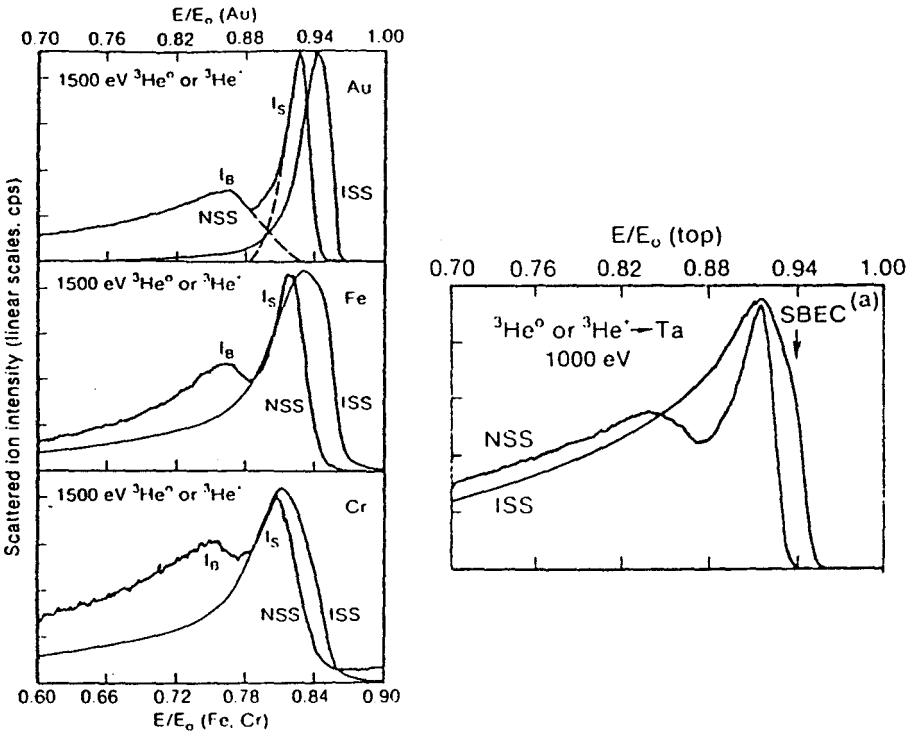

Figure 4.3: NSS and ISS spectra from different targets measured by Thomas et al. [23]. I_S is attributed to scattering from the surface layer, whereas I_B is attributed to sub-surface scattering. The absolute intensities of the NSS and ISS-spectra cannot be compared.

element	He^+ from NSS/ISS at (%)		
	2 keV	1.5 keV	1 keV
Ag	0.74	0.27	0.05
Al	1.9	1.9	2.3
Au	0.5	0.5	0.15
Cr	1.3	0.9	0.4
Cu	0.08	0.04	0.02
Mo	2.5	2.0	1.13
Ni	0.53	0.24	0.06
Pd	1.75	1.17	0.13
Si	0.7	0.9	1.5
Ta	5.3	2.96	1.42
W	4.56	2.96	1.08

Table 4.2: Intensity-ratio of I_S-peak in NSS-spectra and ISS surface-peak at different energies for different targets measured by Thomas et al. [23].

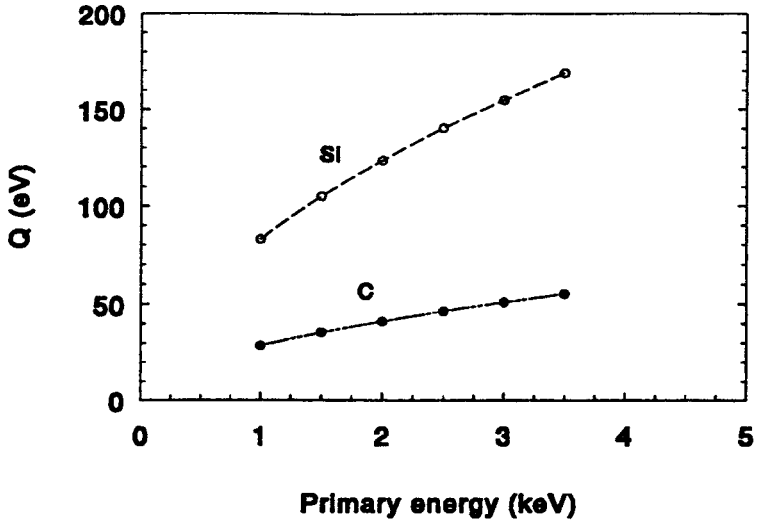

Figure 4.4: Variation of inelastic loss Q with energy due to excitation for He^+ interacting with a C and a Si surface according a theory of Firsov [24].

4.2.2 Peak position

Introduction

In a LEIS spectrum it is, in general, found that the scattering peaks are shifted towards lower energies with respect to the calculated binary collision energy. This inelastic energy loss is due to processes such as excitation, ionization and electron emission.

The inelastic energy loss Q has been calculated without taking into account the exact electronic structure of the interacting particles by Firsov [24]. It is based on transfer of energy and momentum of electrons of the ion to electrons of the surface atom. This inelastic loss is given by:

$$Q[eV] = \frac{(Z_1 + Z_2)^{5/3}\, 4.3 * 10^{-8}\, v}{(1 + 3.1(Z_1 + Z_2)^{1/3}\, 10^7\, b)^5} \tag{4.1}$$

where b [cm] is the impact parameter and v [cm/s] the ion velocity.

The variation of the inelastic loss with energy according to this theory is shown in figure 4.4. As one can see from this figure, the inelastic loss increases with energy and reaches values up to 150 eV for Si.

Results

The measured peak shift to lower energies with respect to the calculated binary collision value, is shown in table 4.3 for 1, 2 and 3 keV incident He^+. As can be seen from this table, the inelastic loss energy can reach values larger than 60 eV. The large errors are due

element	Q (eV) at			element	Q (eV) at		
	1 keV	2 keV	3 keV		1 keV	2 keV	3 keV
Cu	19	27	34	Al	28	35	47
Ni	22	29	34	Si	33	47	58
Pd	24	33	42	Cr	31	40	54
Pt	27	35	44	Mo	32	45	61
Rh	27	39	65	Ta	33	46	49
Ir	23	39	52	W	35	45	52
Ag	20	28	30				

Table 4.3: Peak shift of the LEIS surface-peak to lower energies for 1, 2 and 3 keV He^+ on different elements. The errors are $\pm$ 5 eV at 1 keV, $\pm$ 10 eV at 2 keV and $\pm$ 15 eV at 3 keV.

to the uncertainty of the position of the sample with respect to the analyzer which results in a uncertainty in scattering angle.

Cu, Ni and Ag show the smallest shift and quite similar behavior with energy. Ta, W, Mo, Cr and Si show larger shifts. Since Cu, Ni and Ag have high threshold energies for reionization and Ta, W, Mo, Cr and Si low thresholds, there seems to be a relation between peak shift and reionization probability. To illustrate this, the peak shift has been plotted as function of the threshold for reionization for 1 and 2 keV He^+ incidence in figure 4.5.

To explain the correlation between peak shift and threshold for reionization, the results have to be compared to literature. According to Aono et al. [20] the surface peak in a LEIS spectrum in some cases consists of two peaks which are separated by a constant energy of approximately 20 eV. The high energy peak is attributed to ions that survived neutralization during the whole trajectory. The lower energy peak originates from ions that were neutralized during the incoming trajectory, reionized during the collision and survived neutralization during the outgoing trajectory. The reionization process causes an extra energy loss of $\approx$20 eV.

Therefore, the present result may indicate that for elements with high threshold energies for reionization, such as Ni, Cu and Ag, the peak in a LEIS-spectrum is the result of ions that survived neutralization during the whole trajectory. For elements with low threshold energies such as Al, Si, Cr, Mo, Ta and W, the surface peak probably mainly consists of reionized neutrals, especially at high primary energies. This is in agreement with results of Shoji et al., who observed a single peak and a small peak shift for Ag and Au [25] and two peaks for Si [26], Pb [27] and Ta and W [28]. Thomas et al. [23] conclude that for Cu, Ni, Pd, Ag, Au, Fe, Cd and Co, the scattering peak arises at the predicted energy, whereas for Ta the maximum corresponds to that of reionized neutrals.

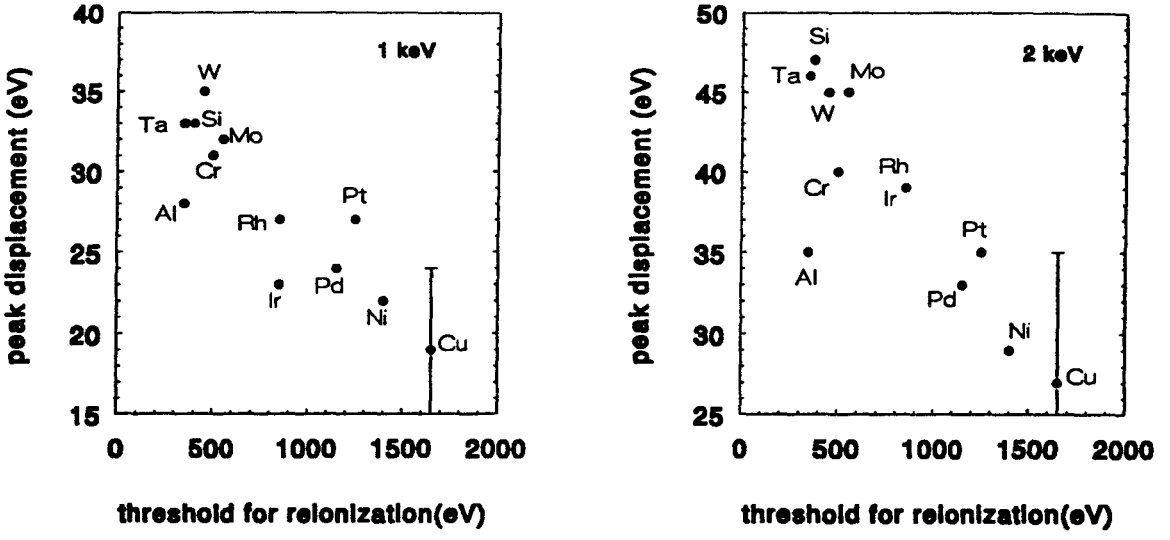

Figure 4.5: Peak-shift of LEIS surface peak with respect to the calculated binary collision energy as function of threshold energy for reionization for 1 and 2 keV He^+ incident on different elements. The error bar indicated for Cu is typical for all elements.

4.2.3 FWHM of the surface peak

Introduction

The Full Width Half Maximum (FWHM) of a peak in a LEIS spectrum is determined by the following factors:

- different isotopes of the target
- transmission behavior of the CMA ($\Delta E/E = c$)
- vibration of surface atoms
- spreading of incident beam energy ΔE or scattering angle $\Delta\Theta$

The most important factor is the transmission behavior of the CMA. The effect of different isotopes in the target is shown in table 4.4 for the elements studied in this work. Especially at low target mass, the energy difference between two main isotopes can be up to 70 eV.

Results

In table 4.5, the measured FWHM of the surface peak in the LEIS-spectra is shown. To illustrate the (a)symmetry of the peak, not only the directly measured FWHM is shown,

element	mass (u)	%	E_f 3 keV He^+	E_f 3 keV Ne^+	element	mass (u)	%	E_f 3 keV He^+	E_f 3 keV Ne^+
Al	27	100	1795	104	Rh	103	100	2625	1524
Si	28	92	1829	128	Pd	104	9	2628	1534
	29	4.7	1860	153		105	22	2631	1545
	30	3.1	1891	179		106	27	2635	1554
Cr	50	4.3	2277	693		108	27	2641	1574
	52	83.3	2301	738		110	13	2647	1593
Ni	58	68	2366	867	Ag	107	51.8	2638	1564
	60	26	2385	907		109	48.2	2644	1584
	61	1.2	2394	926	Ta	181	99.9	2780	2048
	62	3.8	2402	936	W	182	26	2782	2052
	64	1	2419	983		184	30	2784	2061
Mo	92	15	2583	1402		186	28	2786	2069
	94	9	2591	1425	Ir	191	37	2792	2090
	95	16	2595	1437		193	63	2794	2097
	96	17	2599	1448	Pt	194	33	2795	2102
	97	10	2603	1460		196	25	2797	2109
	98	24	2607	1471		198	7	2799	2117
	100	9	2614	1493					

Table 4.4: Effect of different isotopes on the width of LEIS peaks for different targets at 3 keV incident energy (Θ=136°).

element	FWHM (eV) at					
	1 keV		2 keV		3 keV	
	a	b	a	b	a	b
Cu	16	16	25	26	36	36
Ni	18	16	26	26	40	38
Pd	16	14	29	26	43	38
Pt	18	15	26	22	38	37
Rh	18	14	36	28	66	48
Ir	21	16	37	26	64	44
Al	28	26	47	35	71	46
Si	32	32	44	38	65	58
Cr	23	22	43	32	72	44
Mo	28	22	59	36	94	64
Ta	33	28	50	38	60	42
W	34	24	46	34	62	48

Table 4.5: FWHM of LEIS surface-peaks for 1, 2 and 3 keV $^4He^+$ on different elements. The value in column a is the FWHM directly measured, the value in column b is twice the energy difference between the top of the peak and half height on the right side of the peak. The difference between the two values listed can be used as an indication for the symmetry of the peak. The errors are ±5 eV at 1 keV, ±10 eV at 2 keV and ±15 eV at 3 keV.

but also twice the energy difference between the top of the peak and half height on the right side of the peak.

As can be seen from the table, the width of all peaks increases with increasing primary energy.

In spite of the fact that Al and Ta do not have any isotopes, the FWHM is not significantly smaller than for other elements. The behavior of Cu, Ni, Pd and Pt seems to be similar (narrow, symmetric peaks). Si, Ta, W and Mo all have broad, asymmetric peaks. The width of the peaks of Rh and Ir is small at low energies, but rapidly increases with energy. The asymmetry of the peaks is largest for elements with low threshold energies for reionization. This points to, just as in the peak position, a correlation between the FWHM and the threshold for reionization (see figure 4.6).

The observations are consistent with experiments of Shoji et al. [27, 28], who found narrow peaks for Ag and Au and broad peaks for Si, Ta and W. It is obvious from these results that reionization is the most important phenomenon determining the peak-width in He^+-spectra. Reionization causes broadening of the peaks. Furthermore the peaks become more asymmetric. The influence of different isotopes in the target is only visible in the case of Mo, where it causes an extra broadening of the peak.

Assuming the increase of the width with energy for Cu is only due to the transmission

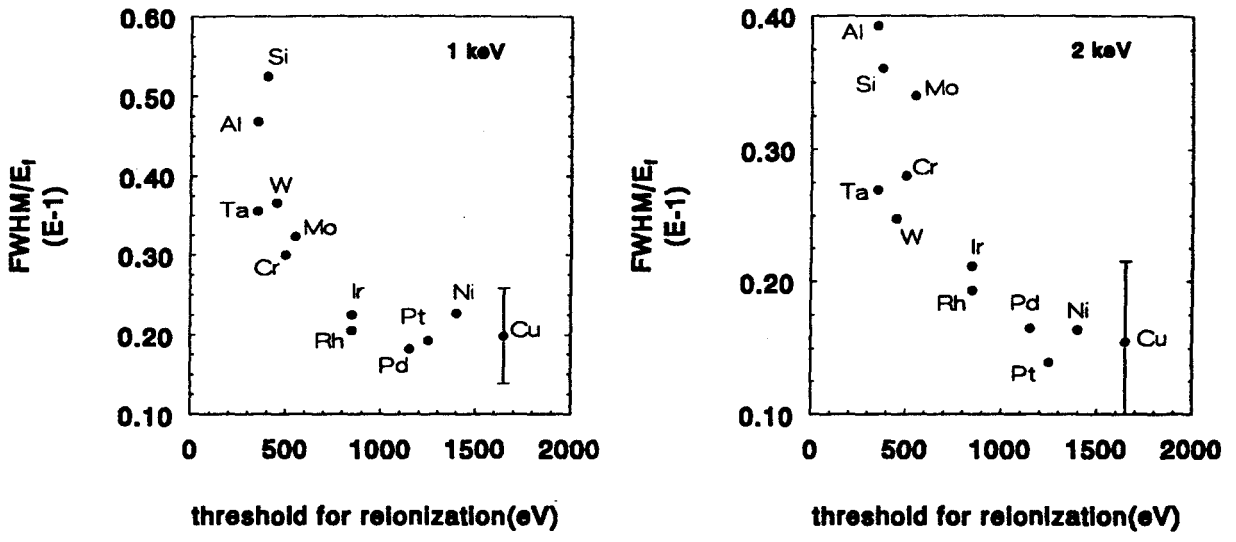

Figure 4.6: FWHM of the surface peak in LEIS-spectra of different elements as function of threshold energy for reionization at 1 and 2 keV He^+ incidence. The width has been divided by E_f to cancel out the influence of the analyzer. The error bar indicated for Cu is typical for all elements.

of the analyzer, the $\Delta E/E$ value is 20/2000=0.01, which is close to the design value for the CMA of the NODUS-machine [21].

4.3 Neutralization of primary ions

Results

According to equation 2.8, the characteristic velocity v_c determines the neutralization of incident ions; the higher the value for v_c, the lower the ion fraction and thus the higher the neutralization.

The characteristic velocity for different elements has been determined by measuring the LEIS signals at 1.0, 1.5, 2.0, 2.5, 3.0 and 3.5 keV $^3He^+$and $^4He^+$ incidence on the particular element and plotting $\ln(S/\frac{d\sigma}{d\Omega}IE_f) = \ln(cP^+)$ against $\frac{1}{v_i} + \frac{1}{v_f}$ (see equations 2.2 and 2.8). The value for v_c then follows from the slope of this line. In figure 4.7, an example of the determination of v_c for different elements is shown.

As one can see, the linear relationship predicted by the theory is found with good accuracy for practically all targets. Only for Cu, some deviation from the theory is found. A similar behavior was found for Zn [29] and Ag [30].

It will be shown in appendix A, that differences in characteristic velocities are more easily determined than absolute values. In table 4.6, the values for v_c (directly measured and with respect to Pd, the lowest measured value for v_c) for different targets are shown. In this

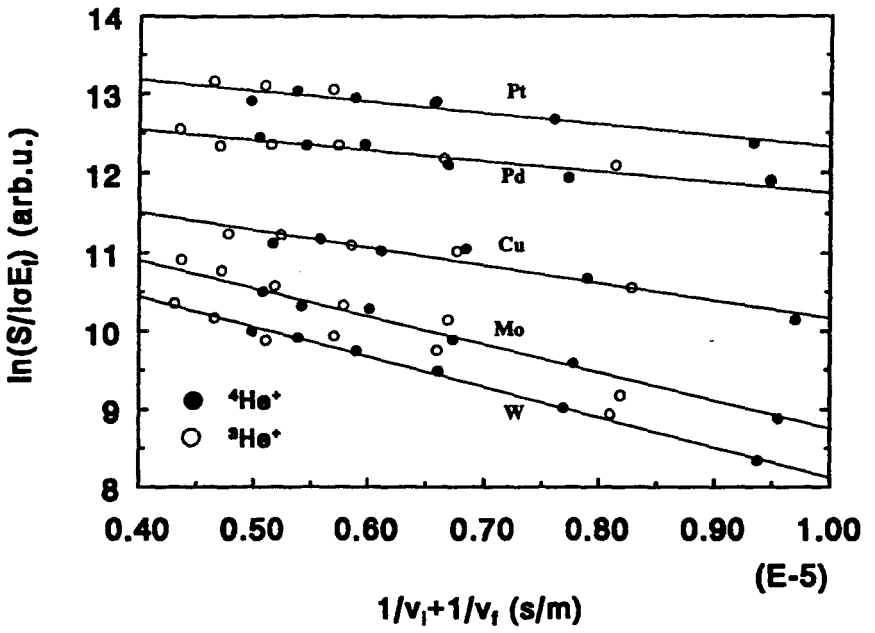

Figure 4.7: *ln* of the LEIS-signal divided by cross section, final energy and beam current as function of the sum of the reciprocal velocities. For clarity, the lines have been shifted vertically.

table, also characteristic parameters describing the electronic structure of the target, such as electronic configuration, workfunction [31] and valence band width [33] are listed. The valence band-width is defined as the energy difference between the bottom of the valence band and the Fermi energy. This has been done because O'Connor et al. [14] evaluated the role of these electronic parameters on the neutralization behavior. A correlation was found between the measured v_c and the band width of the target. This indicates that neutralization is enhanced when the energy difference between the bottom of the valence band and the ground state of the He ion is smaller.

The v_c-values measured in this work show no clear correlation with workfunction (see table 4.6). For example, Mo and Cu have similar workfunction values but completely different values for v_c. Also no correlation is found with band width, which can be seen from Al, Pt and Pd, Mo which have similar values for the bandwidth but a large difference in v_c. There seems to be some correlation between the electronic configuration and the measured characteristic velocity: the higher the number of filled d-states, the lower the value for v_c. This correlation will be discussed in more detail in the next paragraph.

Absolute ion fractions can be calculated using equation 2.8 and the measured values for v_c (see figure 4.8). According to the theory and the v_c values from table 4.6, the ion fraction is lowest for 1 keV He^+ on Si ($\approx$ 1 %) but can reach values up to 60 % for 3.5 keV He^+ on Pd. There is a wide spread in absolute ion fractions depending on both target and primary energy of the ion.

element	conf.	workf. (eV)	B.W. (eV)	v_c (10^5 m/s)	$v_c - v_c^{Pd}$(10^5 m/s)
Al	$3s^2p^1$	4.28	11.2	3.8±0.3	2.5±0.4
Si	$3s^2p^2$	4.85	12.5	4.8±0.3	3.5±0.4
Ta	$5d^36s^2$	4.25	7.8	3.4±0.3	2.1±0.4
W	$5d^46s^2$	4.55	10.1	3.8±0.3	2.5±0.4
Cr	$3d^54s^1$	4.50	7.8	3.7±0.3	2.4±0.4
Mo	$4d^55s^1$	4.91	7.3	3.8±0.3	2.5±0.4
Ir	$5d^76s^2$	5.27	11.1	3.4±0.3	1.1±0.4
Rh	$4d^85s^1$	4.98	7.5	1.6±0.2	0.3±0.3
Ni	$3d^84s^2$	5.22	9.4	1.8±0.2	0.5±0.3
Pt	$5d^86s^2$	5.65	10.8	1.5±0.2	0.2±0.3
Cu	$3d^{10}4s^1$	4.65	9.4	2.0±0.4	0.7±0.5
Pd	$4d^{10}$	5.12	7.3	1.3±0.1	0

Table 4.6: Values for v_c (directly measured and with respect to Pd) and electronic properties (electronic configuration, workfunction [31] and valence band-width [33]) for the different targets.

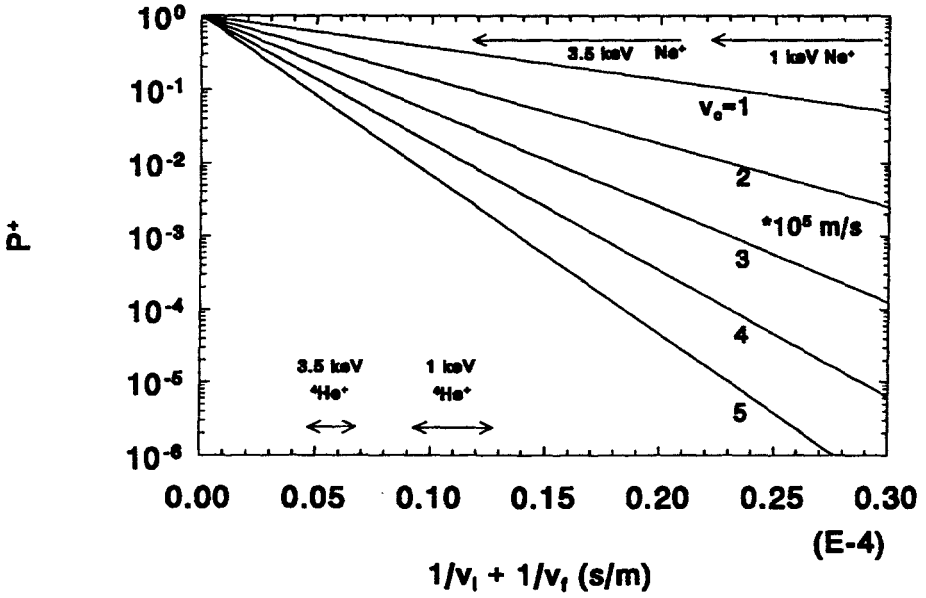

Figure 4.8: Ion fraction as function of the sum of the reciprocal velocities for different characteristic velocities according to Hagstrum's theory [5]. The arrows indicate the $1/v_i + 1/v_f$-range for scattering of an ion from different targets.

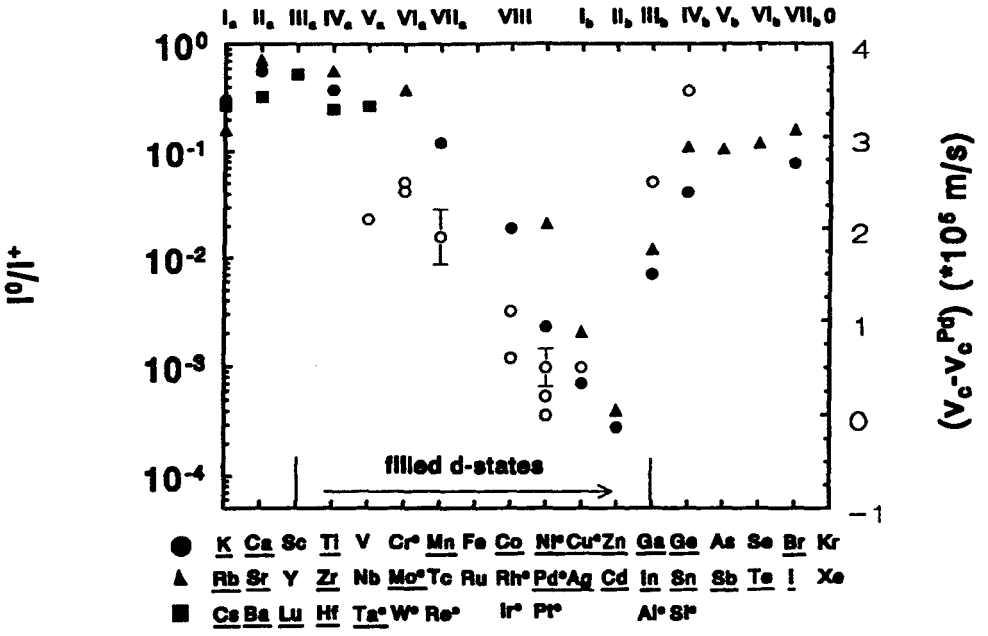

Figure 4.9: Comparison between ionization probabilities measured by Souda et al. [32] (closed symbols) and differences in characteristic velocities (as a measure for neutralization) measured in this work (open circles).

4.4 Qualitative model for the He^+-results

The correlation between the electronic configuration and the measured characteristic velocity, as described in the previous section, can also be interpreted as a correlation between the reionization probability and v_c since Aono et al. [20] found that the threshold energy for reionization increases with the number of filled d-states.

To illustrate this, the v_c-values are plotted in figure 4.9 in the same plot as ionization probabilities measured by Souda et al. [32]. Another way to show the correlation is to plot v_c as function of the threshold energy for reionization (obtained from table 4.1) see figure 4.10.

The explanation for this observation can be given on the same basis of level crossing as was developed to explain reionization [32]. Figure 4.11 presents the diagram of He^+, M^- and He^0, M, modified to include a possible neutralization process. At close distances, crossing of the levels provides the possibility of forming a quasimolecule "HeM":

$$He^+ + M^- \rightleftharpoons "HeM" \rightleftharpoons He^0 + M$$

The level crossing and formation of a quasimolecule provide the possibility of both neutralization and ionization at the close encounter. The possibility for level crossing and the formation of a quasimolecule seems to depend on the number of filled d-states.

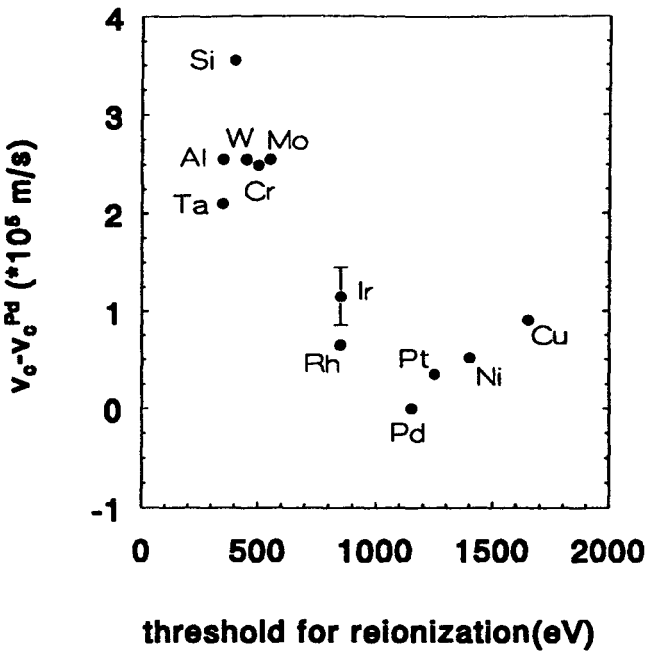

Figure 4.10: Correlation between neutralization and reionization: differences in measured characteristic velocities against threshold energies for reionization.

For a quantitative explanation of the observed correlation in the behavior of v_c (or P^+) and the reionization for different elements, quantum-mechanical calculations would be needed, for example, as in the Muda-Newns approach [34]. Qualitatively, we can analyze this correlation on the basis of the three stage model proposed by Verhey et al. [13], later supported by O'Connor et al. [14], Rabalais et al. [16] and Souda et al. [7]. According to this model, the interaction between projectile and target atom can be divided into three parts:

1. an incoming trajectory where (Auger) neutralization may occur

2. a close encounter where reionization and additional neutralization can take place

3. an outgoing trajectory where (Auger) neutralization can occur

Since the stages are considered to be independent, the measured fraction (P^+) can be expressed as:

$$P^+ = (1 - N^{in})(1 - N^c)(1 - N^{out}) + N^{in} I^c (1 - N^{out}) \tag{4.2}$$

where $N^{in,out}$ is the probability for (Auger) neutralization during the in and outgoing trajectory, and I^c (N^c) is the probability for ionization (neutralization) at the close encounter.

We can assume that $N^{in} = N^{out} = N$ because, especially for heavy target atoms, the difference between initial and final velocities of the projectile (He^+) is small. According

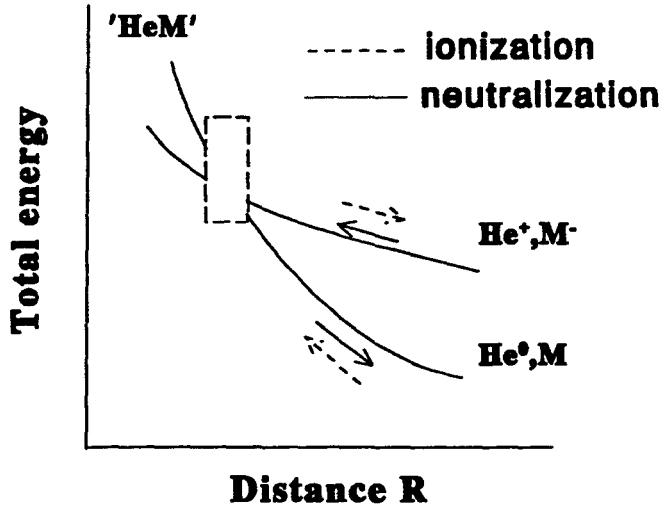

Figure 4.11: Schematic figure showing the mechanism of reionization and neutralization.

to the experimental data, the ion fraction is significantly smaller for elements with empty d-states (P_1^+) than for elements with filled d-states (P_2^+). Equation 4.2 then gives:

$$(1-N)^2(1-N_1^c) + NI_1^c(1-N) << (1-N)^2(1-N_2^c) + NI_2^c(1-N) \tag{4.3}$$

According to Souda et al. [32] $I_1^c << I_2^c$ (see figure 4.9). We can then write:

$$(1-N)(N_1^c - N_2^c) >> NI_1^c \tag{4.4}$$

Further comparison is difficult because the relative contributions of Auger neutralization and neutralization at the close encounter are unknown. However, according to this simple model, N_1^c must be greater than N_2^c, and thus the degree of neutralization *at the close encounter* is higher for target elements which have higher probabilities for ionizing of He^0 [38].

4.5 Level shift and broadening

4.5.1 Level shift

As described in the previous section, level crossing is very important process determining the charge exchange processes between projectile and target atom. The shift of the individual levels is the result of bonding or anti bonding interaction of the He 1s orbital and the surface valence orbitals. The level shift was used in reference [34] to calculate ionization probabilities for $He^+ \rightarrow$Si and $He^+ \rightarrow$Cu interactions. The authors used an upward shift of He 1s level of about 23.7 eV when interacting with Si and a downward shift of 4.4 eV [35] for $He^+ \rightarrow$Cu resulting in an ionization probability at 1 keV He^+ incidence

that is approximately 40 times larger for Si than for Cu [35]. The level shift was thus found to be one of the most important factors concerning reionization.

We can estimate the shift of a single level (for example the He-1s level) when approaching a target atom by constructing a separated-united atom diagram [16, 27] following the rules of Barat et al. [39]. This model assumes that the separated atoms (having nuclear charges Z_1 and Z_2) form a united atom (having a nuclear charge $Z = Z_1 + Z_2$) at small distances: Molecular orbitals connect the levels of infinitely separated atoms with these of the united atom.

For the interaction of He^+ with the metals studied in this work these diagrams have been constructed (figure 4.12). The energy level data were obtained from Hartree-Fock calculations [40].

According to these diagrams, the He 1s level shifts to lower binding energies when approaching a target atom. Only for Cu, a shift to higher binding energies is found.

4.5.2 Level broadening

Besides shifting of the level, also broadening will occur as the ion approaches the surface. The broadening can be related to the finite lifetime of the level by the uncertainty principle [41], and thus to the transition probability: if the transition probability for neutralization (i.e. for filling of the state) is R, the lifetime of the state is $1/R$. The energy broadening or uncertainty Γ can then be written as:

$$\Gamma = \hbar R \tag{4.5}$$

where R is given by $R = A\exp(-as)$ (chapter 2). Typical values for a, determining the ion-surface interaction range, are 2–6 $Å^{-1}$ [5, 16]. Since $A/a = v_c \approx 2 * 10^5$ m/s, typical values for A are $8*10^{15}$ s^{-1}. Using these values, the level broadening as function of the distance between ion and surface can be calculated (figure 4.14).

Typical values for the distance of closest approach are 0.1–0.3 Å (see figure 2.6). According to this model, the level broadening is then between 1 and 5 eV.

4.6 Conclusions

The effect of the target on the shape of a LEIS-spectrum and on the neutralization behavior was studied for He^+-scattering [38] from a number of pure metals. The energy position of the surface peak indicates that for elements with high threshold energies for reionization, the surface peak probably mainly consists of ions that survived neutralization during the incoming trajectory, close encounter and outgoing trajectory. For elements with low threshold energies for reionization the surface peak is probably mainly due to ions that were neutralized during the incoming trajectory, reionized at the close encounter and survived neutralization during the outgoing trajectory.

Characteristic velocities determining the neutralization of noble gas ions were measured for a number of pure elements. No clear correlation was observed between these v_c-values

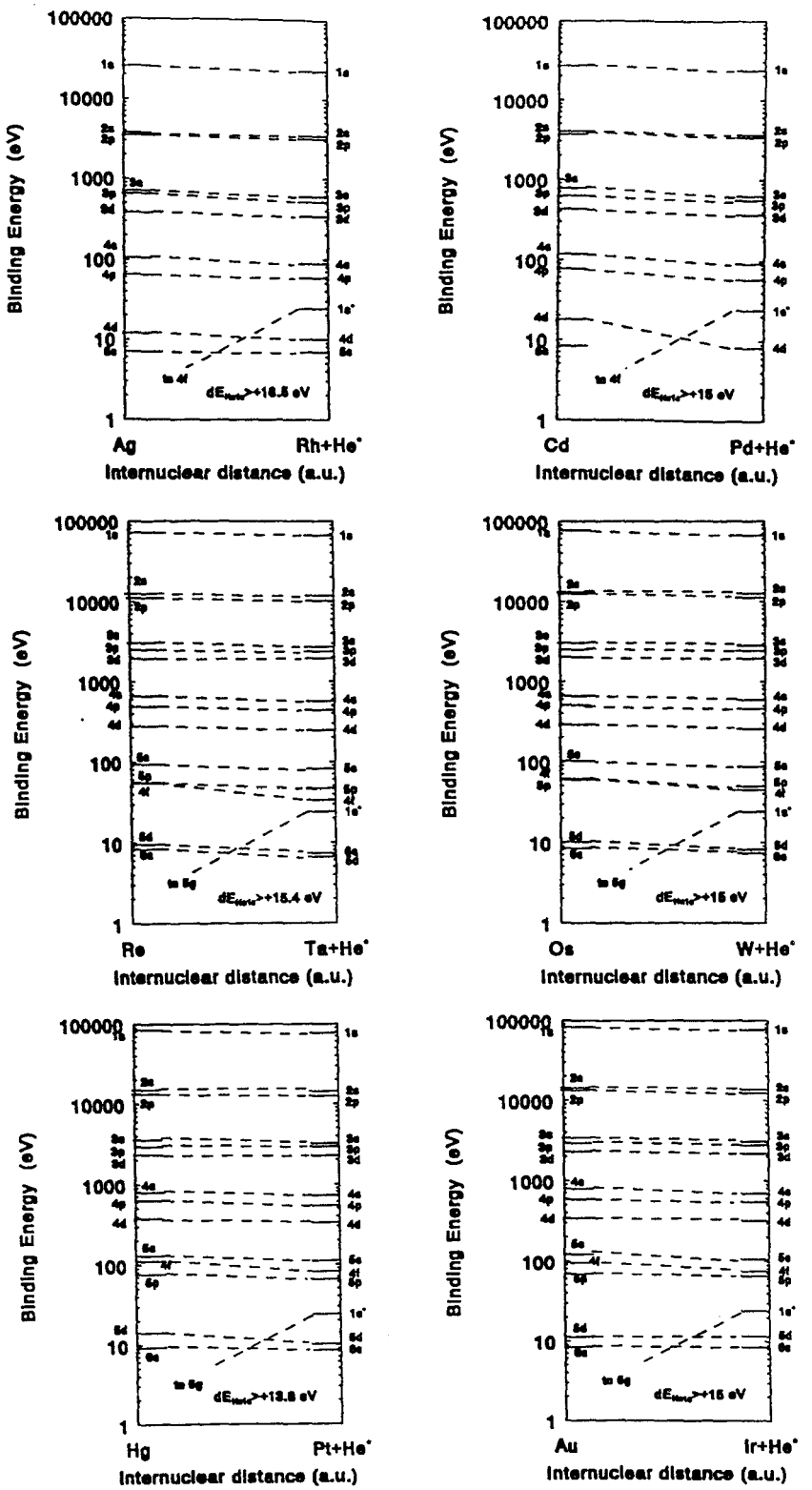

Figure 4.12: Separated-united atom correlation diagrams for He on the metals studied in this work. Molecular orbitals (MO) connect the levels of the infinitely separated atoms (right-hand side) with those of the united atom (left-hand side), maintaining the same value of quantum number difference (n-l).

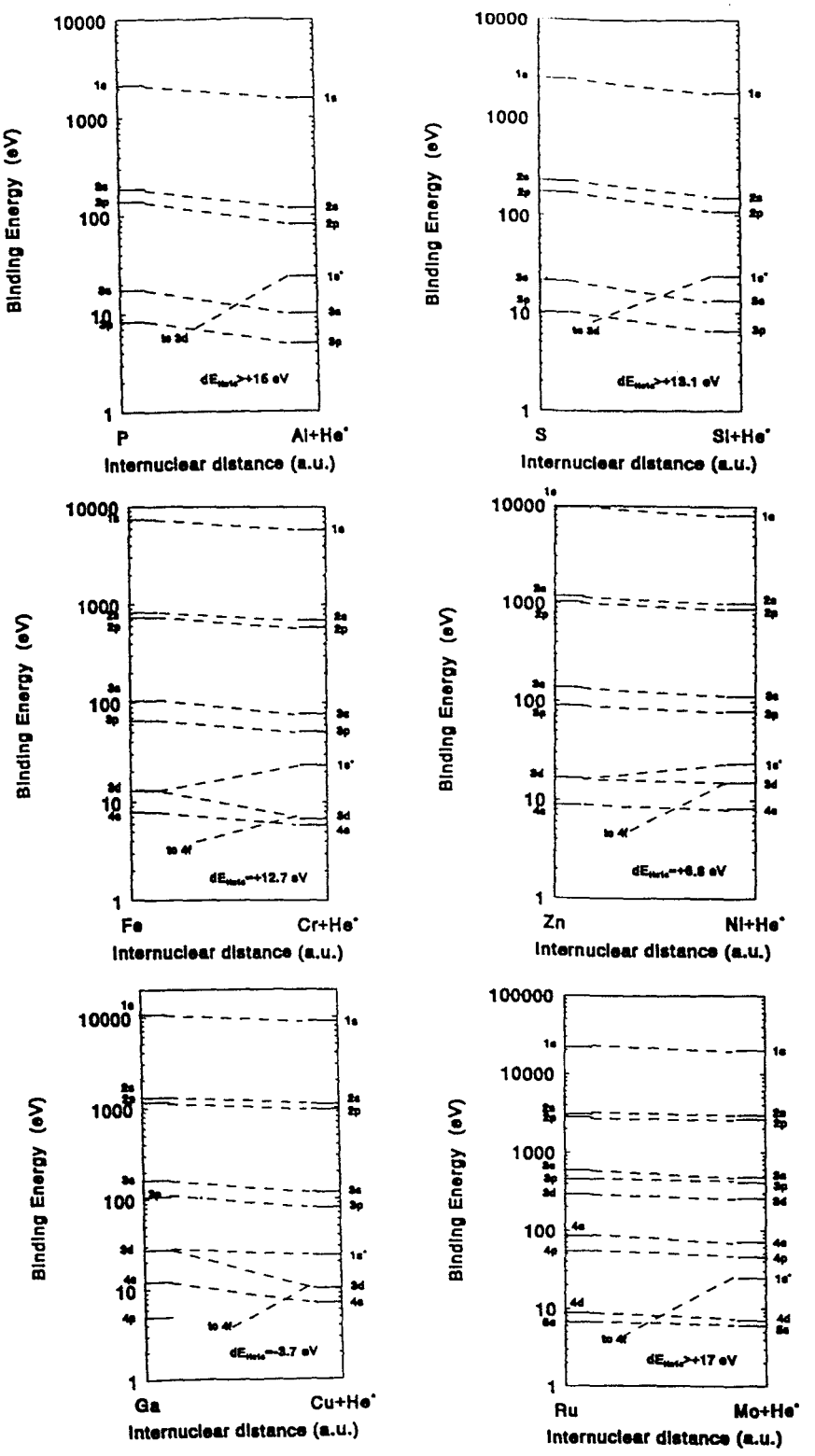

Figure 4.13: Separated-united atom correlation diagrams for He on the metals studied in this work. Molecular orbitals (MO) connect the levels of the infinitely separated atoms (right-hand side) with those of the united atom (left-hand side), maintaining the same value of quantum number difference (n-l).

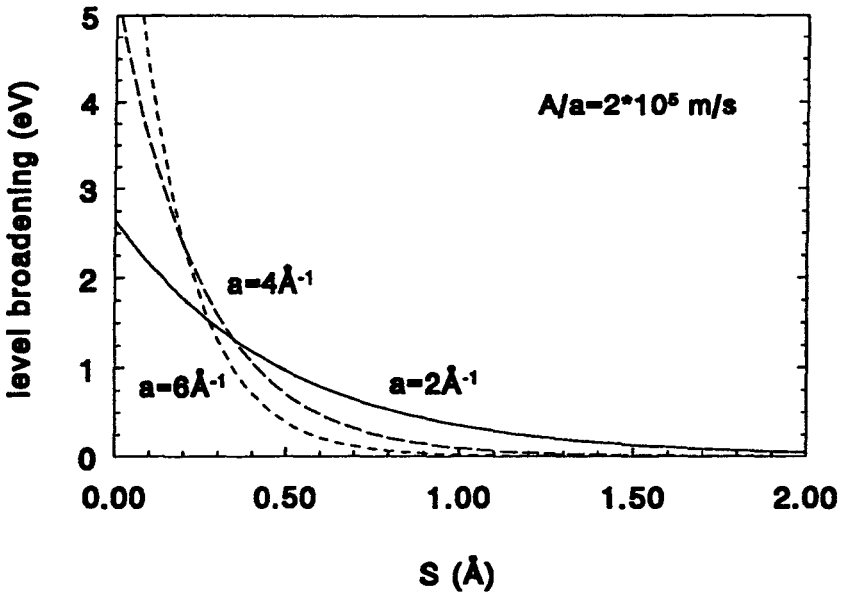

Figure 4.14: Level broadening due to the finite lifetime of the level as function of the distance between ion and surface.

and workfunction or valence band width of the target. The neutralization behavior was found to be strongly dependent on the position of the element in the Periodic Table. Neutralization is suppressed for elements with filled d-states (and thus for elements with small reionization probabilities). The observed correlation between neutralization and reionization was qualitatively explained by a level crossing model. The shift of the He-1s level when approaching a target atom, was thus found to be one of the most dominating factors determining the charge exchange processes.

In order to obtain a more quantitative explanation for the observed behavior, quantum-mechanical calculations are currently performed, as in the Muda-Newns approach [34].

Chapter 5

Low-Energy Ion Scattering from Alloys

5.1 Introduction

In the previous chapter, the LEIS results on various pure metals were discussed. The aim of that work was to study the effect of target atom on the LEIS signal, which is important for direct quantification.

Quantitative analysis of, for example, metal alloys is possible in many practical cases with calibration against pure elements: the ratio of the signal of element i in the alloy and the signal of the pure element i, measured under identical experimental conditions, is directly the ratio of atoms at the surface in the alloy and pure element (see equation 2.2), provided that the neutralization behavior (P^+) is independent of the chemical environment (no matrix effects). The opinion in literature about possible matrix effects is controversial. On the one hand, Novacek et al. [44] and Ackermans et al. [45] reported the absence of matrix effects in NiPt and CuPd alloys. However, strong matrix effects were observed for He^+ scattering from different carbon species [37]. Currently, the absence or presence of matrix effects in LEIS cannot be predicted.

In order to test the calibration method, three alloys, $Ni_{80}Pt_{20}$, NiAl(110) [42] and $Ag_{80}Al_{20}$ have been measured using $^4He^+$ and $^3He^+$ at various incident energies (corresponding to different ion fractions). As calibration samples, a Ni(100) single crystal, an Al polycrystalline sample and a Pt polycrystalline ribbon were used. The Ag pure elemental data were taken from reference [30]. If no matrix effects are present, the measured composition of the alloy should be the same at each energy.

NiPt alloys are technologically important because of their catalytic properties. An advantage of this alloy is that Ni and Pt can form Ni_xPt_{1-x} random solid solution alloys at all concentrations x.

NiAl(110) is known to be an ordered alloy with a stable, well characterized surface. This makes it ideal to be used as a model system. Furthermore, the corrosive resistance of NiAl is better than steel. An other property of NiAl(110) is the formation of a thin Al_2O_3 layer

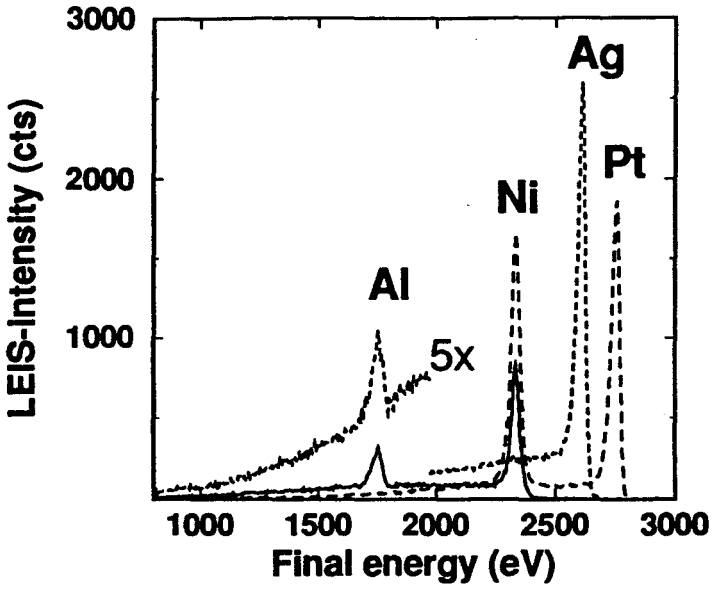

Figure 5.1: 3 keV $^4He^+$ LEIS spectrum of the three alloys studied in this work.

on top of the crystal after oxidation. Al_2O_3 is often used as a support for catalytically active components. Stef Reijne [43] performed LEIS-measurements on different Al_2O_3 surfaces.

Some AgAl alloys were measured by Dirks et al. [47]. An interesting feature of these alloys with an Al concentration < 15 %, is a change in the surface structure at some temperature, probably due to a phase transition [47].

An advantage of the calibration method is that an ion, scattered from a specific element (in the pure or alloy sample) passes the analyzing and detection system with the same final energy. In this way, no correction has to be applied for transmission of the CMA or efficiency of the channeltrons. An example of a LEIS-spectrum of the three alloys is given in figure 5.1.

5.2 Results

5.2.1 $Ni_{80}Pt_{20}$

The concentrations of Ni and Pt obtained from the LEIS signals at different energies are shown in figure 5.2.

As one can see, the concentrations are, within the experimental error, constant in this energy range: 34±3 % Pt and 65±4 % Ni, which adds up to a total of 99 %. The obtained surface structure deviates significantly from the bulk structure (80 % Ni, 20 % Pt). This is probably due to preferential sputtering of Ni atoms during the Ar^+ bombardment cleaning procedure. A similar Pt enrichment was found by Novacek et al. [44].

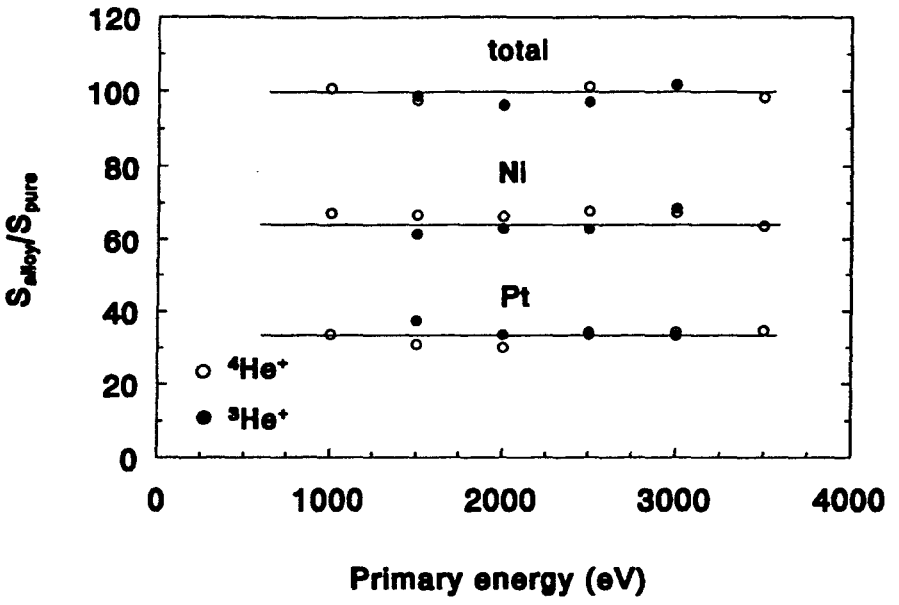

Figure 5.2: Measured Ni and Pt concentration of a $Ni_{80}Pt_{20}$ alloy as function of the incident energy.

5.2.2 $Ag_{80}Al_{20}$

The measured Ag and Al concentrations in the $Ag_{80}Al_{20}$ are shown in figure 5.3.

The concentration seems to be independent of the incident energy. Furthermore the measured concentrations (81±5 % Ag and 18±3 % Al) reflect the bulk composition and add up to 100 %.

An interesting feature of AgAl-alloys having Al-concentrations < 15%, is a change in the surface composition at a certain temperature, probably due to a phase transition [47]. The surface composition of a $Ag_{90}Al_{10}$ alloy has also been determined at two different temperatures. The change in surface structure was indeed observed, as can be seen from figure 5.4. However, due to several experimental problems, listed below, it was found to be difficult to quantify the composition:

- due the uncertainty in the temperature measurement (pyrometer) it was very difficult to get the same conditions
- the time to reach an equilibrium at the surface was unknown
- due to the small Al signal, a long measuring time was needed in order to allow an accurate determination of the area of the surface Al peak. However, the Al in the low temperature condition was found to be sputtered easily with the primary ion beam

Since the change of the surface structure was not that important for this work, no effort was put in to solve the experimental problems.

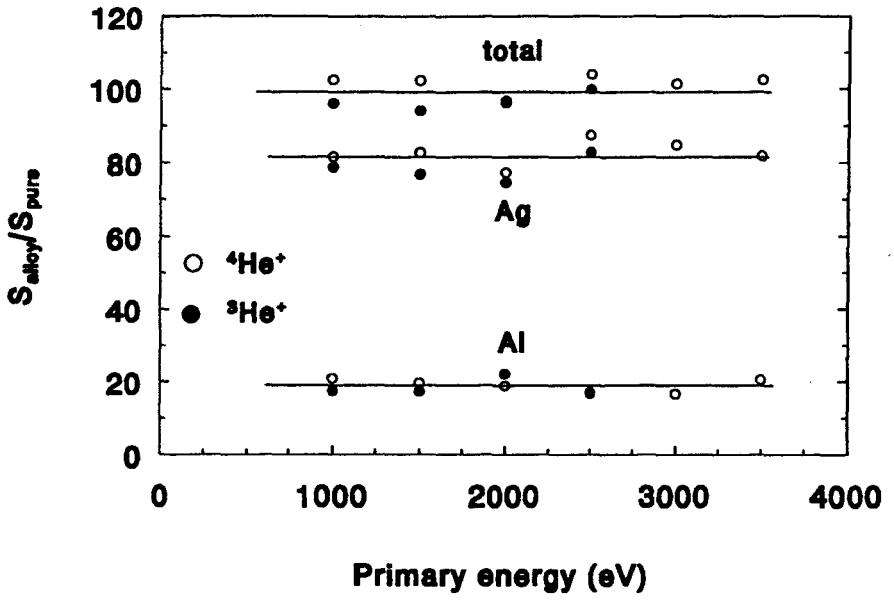

Figure 5.3: Measured Ag and Al concentration in $Ag_{80}Al_{20}$ alloy as function of incident energy.

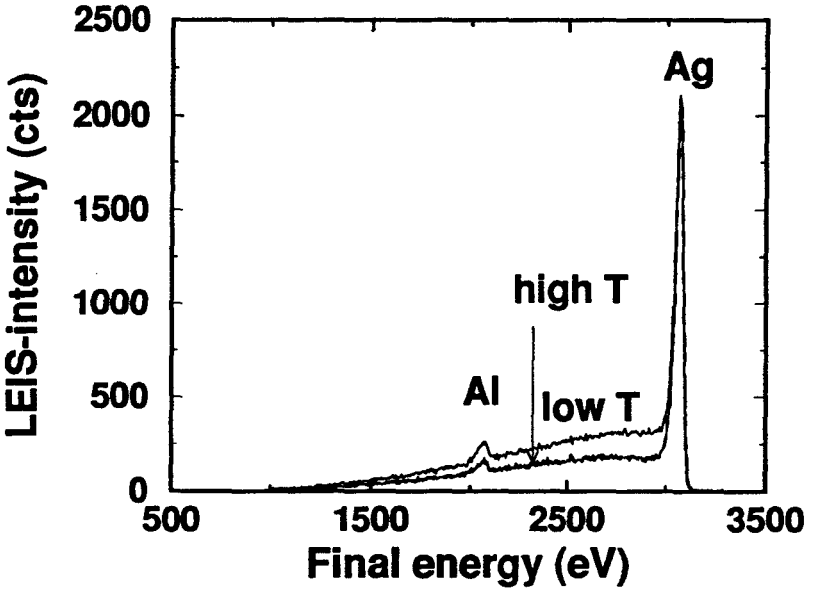

Figure 5.4: LEIS spectrum of an $Ag_{90}Al_{10}$ alloy at two different temperatures ($\approx$ 500°C and $\approx$200°C).

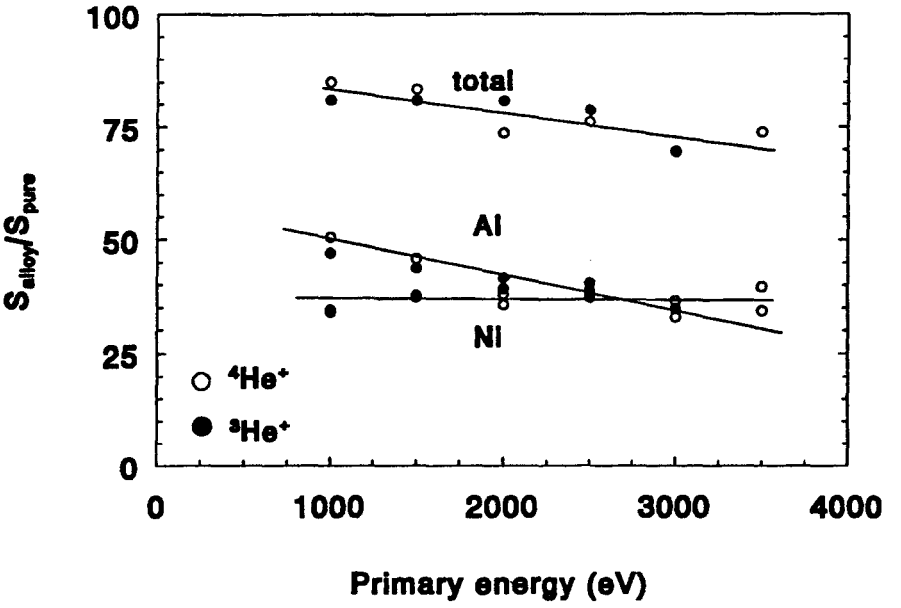

Figure 5.5: Measured Ni and Al LEIS signal ratios in NiAl(110) and pure elements as function of incident energy.

5.2.3 NiAl(110)

The ratios of Ni and Al LEIS signals in the NiAl(110) and the pure elements at different incident energies are shown in figure 5.5.

Since the density of atoms at the surface in the NiAl(110) is different from that of the reference samples (NiAl(110) is a very open structure [46]) the numbers cannot directly be used as a concentration. The calibrated Ni signal is, within the experimental error, constant with energy while the calibrated Al signal decreases with energy.

5.3 Discussion

The use of the calibration method seems to be justified for NiPt and AgAl alloys. For NiAl(110) however the measured composition at the surface seems to depend on the incident energy of the ion.

A possible explanation would be shielding of Al by a contamination (such as H) during the measurement. This effect would however cause the Al signal to increase with increasing energy, since at higher incident energy the shadow cone is smaller (less shielding).

An other possibility would be (because NiAl(110) is a very open structure) contributions from deeper layers to the surface peak. However if this would be the case, both metal signals would have to be affected equally because NiAl has a 1:1 composition at both first and second atomic layer.

A possible explanation for the behavior of Al is a change in neutralization behavior

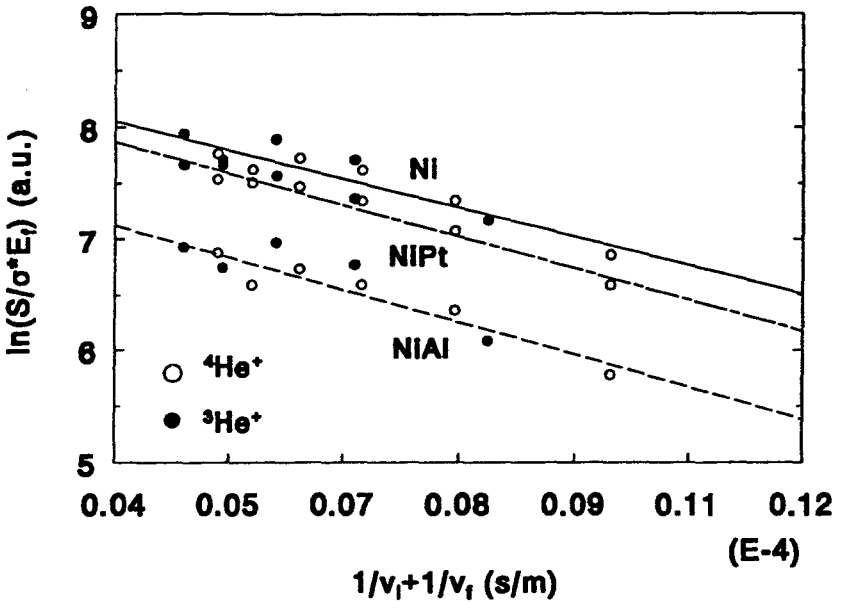

Figure 5.6: Determination of v_c from a plot of the logarithm of signal divided by cross section and final energy as function of the sum of the reciprocal velocities for Ni in Ni(100), $Ni_{80}Pt_{20}$ and NiAl(110). The fact that the lines have the same slope indicates the same neutralization behavior for Ni in different chemical environments.

(matrix effects). This is shown in figures 5.6 and 5.7 where 'characteristic velocity plots', described in the previous chapter, are shown for Ni in both NiPt and NiAl and for Al in AgAl and NiAl.

As one can see, the value for v_c, obtained from the slope of the lines, is smaller for the Al in NiAl than for the pure Al, which indicates less neutralization in the alloy.

The explanation for the change in neutralization behavior might be found in a difference of the electronic structure between pure Al and NiAl. The electronic density of states for the pure elements [33], NiPt [48] and NiAl(110) [49] is schematically shown in figure 5.8.

As can be seen from this figure, the difference in electronic structure between Ni, Pt and NiPt is not very large. The NiAl DOS shows a localized d-band just below the Fermi level, whereas the pure Al has a broad s-p distribution.

As discussed in the previous chapter, the existence of a low energy tail in LEIS spectra might be an indication for level crossing between He and the target. One could imagine, that if crossing occurs, a change in electronic structure can affect the charge exchange processes. However, no matrix effect was observed in Al_2O_3 [50], where also the electronic structure is different from that of the pure Al. A more thorough and detailed theoretical investigation, currently underway, is needed to give a conclusive answer on this subject.

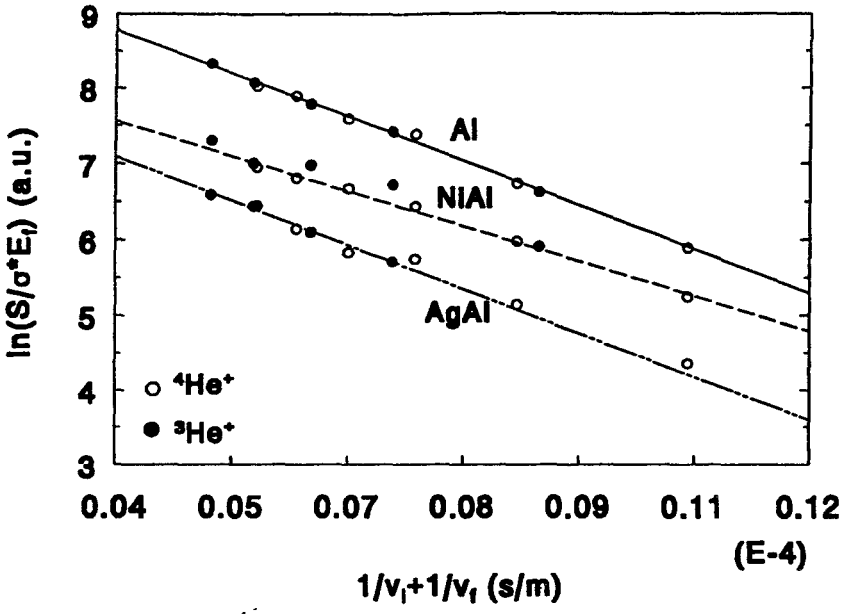

Figure 5.7: Determination of v_c from a plot of the logarithm of signal divided by cross section and final energy as function of the sum of the reciprocal velocities for Al in Al-pure, NiAl(110) and $Ag_{80}Al_{20}$. The different slope for NiAl indicates a change in neutralization of He^+ when scattering from th Al atom.

5.4 Conclusions

The composition of $Ni_{80}Pt_{20}$, NiAl(110) and $Ag_{80}Al_{20}$ alloys was determined using the calibration against pure elements. No matrix effects were observed for $Ni_{80}Pt_{20}$ and $Ag_{80}Al_{20}$. The compositions were measured to be 65±4 % Ni and 34±3 % Pt for the NiPt alloy and 81±5 % Ag and 18±3 % Al for the AgAl alloy. The Pt-enrichment at the surface compared to the bulk observed for the NiPt alloy, is probably due to preferential sputtering of Ni atoms.

For NiAl(110) a change in the neutralization was observed for Al compared to Al pure. For Ni, no change in neutralization was found when changing the environment from Ni pure to a NiAl alloy. At present, no satisfactory explanation can be given for this observation.

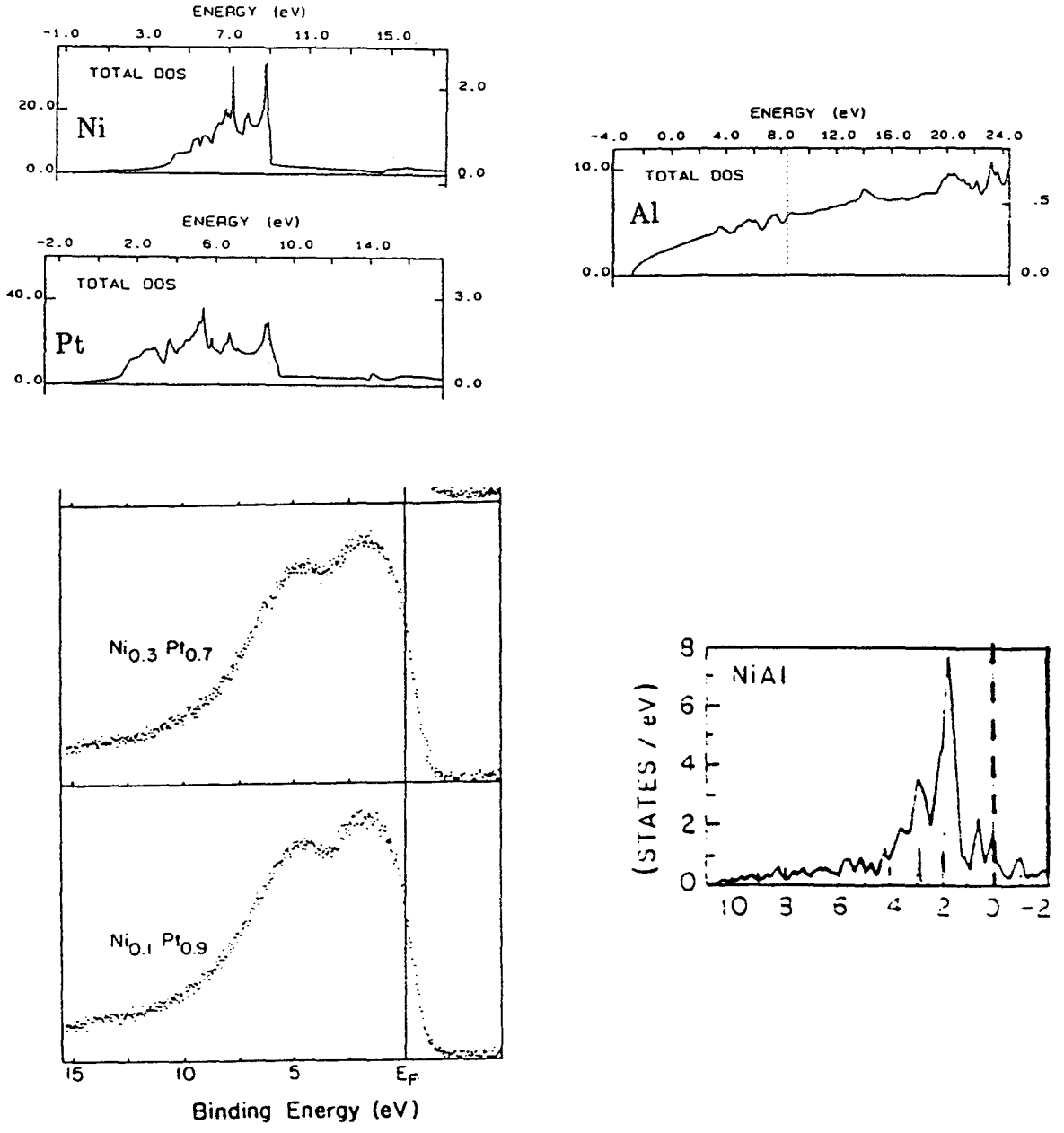

Figure 5.8: Electronic density of states for Ni, Pt and Al pure [33], NiPt [48] and NiAl(110) [49].

Chapter 6

Conclusions and recommendations

In this work, the influence of the chemical environment on the LEIS-signal is studied. Therefore, a number of metals and alloys have been investigated in detail.

For the metals, both the shape of the spectrum and the neutralization behavior can give additional information about the charge exchange processes between the incoming He-ion and the target atom. It was found that the neutralization behavior (experimentally determined from the characteristic velocity) is strongly connected to the reionization behavior (experimentally determined from the threshold energy).

From the experiments and literature it is found that the position of the target element in the periodic table rules the charge exchange processes. The probability for neutralization and ionization is higher for elements with empty d-states than for elements with filled d-states. This can be explained by a level crossing model, which provides the possibility of both neutralization and ionization. The probability for level crossing seems to depend on the number of filled d-states.

To be able to quantify the observed behavior, more thorough quantum-mechanical have to be performed. First attempts found in literature are based on the theory introduced by Muda and Newns [34]. The experimental data presented in this work, in combination with Time Of Flight (TOF)-experiments, which allows a direct measurement of the ion fraction by detecting both neutrals and ions, will be helpful to test these theories.

The use of calibration standards, mostly pure metals, to quantify the surface composition with LEIS has been tested on three alloys. The results are presented in such a way that no correction has to be applied for the analysis and detection system. The results show that the calibration method is a very powerful tool for accurate quantification, provided the chemical environment (matrix) does not influence the neutralization behavior.

However, for NiAl(110), a pronounced decrease in the neutralization for the Al was observed for the alloy compared to a pure Al sample. Therefore, quantification of the surface composition of NiAl (110) was not possible. This might be attributed to a change in electronic structure due to the alloying.

The calibration method allows accurate, easy quantification of the surface composition, but the occurrence of matrix effects cannot be predicted and should therefore always be

checked. This not only holds for alloys, but also for other systems, such as carbon species and oxides.

Bibliography

[1] H. Niehus, W. Heiland, E. Taglauer, Surf. Sci. Rep. **17**, 213 (1993)

[2] H.H. Brongersma and G.C. van Leerdam in *Fundamental Aspects of heterogeneous catalysis studied by particle beams*, eds. H.H. Brongersma and R.A. van Santen, NATO ASI Series B 265 (Plenum Press, New York, 1991) p. 283

[3] I.M. Torrens, *Interatomic potentials* (Academic Press, New York, London 1972)

[4] J.S. Risley, Rev. Sci. Instrum. **43**, 95 (1972)

[5] H.D. Hagstrum, Phys. Rev. **96**, 336 (1954)

[6] H.H. Brongersma and T.M. Buck, Nucl. Instr. Meth. **132**, 559 (1976)

[7] R. Souda and M. Aono, Nucl. Instr. Meth. Phys. Res. B **15**, 114 (1986)

[8] R. Souda, T. Aizawa, K. Miura, C. Oshima, S. Otani and Y. Ishizawa, Nucl. Instr. Meth. Phys. Res. B **33**, 374 (1988)

[9] D.P. Smith, Surf. Sci. **25**, 171 (1971)

[10] M. Beckschulte and E. Taglauer, Nucl. Instr. Meth. Phys. Res. B **78**, 29 (1993)

[11] T.M. Buck, W.E. Wallace, R.A. Baragiola, G.H. Wheatley, J.B. Rothman, R.J. Gorte, J.G. Tittensor, Phys. Rev. B **48** (2), 774 (1993)

[12] R.S. Bhattacharya, W. Eckstein and H. Verbeek, Surf. Sci. **93**, 563 (1980)

[13] L.K. Verhey, B. Poelsema and A.L. Boers, Nucl. Instr. Meth. **132**, 565 (1976)

[14] D.J. O'Connor, Y.G. Shen, J.M. Wilson and R.J. MacDonald, Surf. Sci. **197**, 277 (1988)

[15] R.J. MacDonald and D.J. O'Connor, Surf. Sci. **124**, 423 (1983)

[16] J. Wayne Rabalais, Jie-Nan Chen, R. Kumar and M. Narayana, J. Chem. Phys. **83** (12), 6489 (1985)

[17] T.M. Buck, Y.-S. Chen and G.H. Wheatley, Surf. Sci. **47**, 244 (1975)

[18] W. Eckstein, V.A. Molchanov and H. Verbeek, Nucl. Instr. Meth. **149**, 599 (1978)

[19] G.C. van Leerdam, K.-M.H. Lenssen and H.H. Brongersma, Nucl. Instr. Meth. Phys. Res. B **45**, 390 (1990)

[20] M. Aono and R. Souda, Nucl. Instr. Meth. Phys. Res. B **27**, 55 (1987)

[21] H.H. Brongersma, N. Hazewindus, J.M. van Nieuwland, A.M.M. Otten and A.J. Smets, Rev. Sci. Instrum. **49**, 707 (1978)

[22] E. Pierson, J.-M. Beuken and P. Bertrand, Nucl. Instr. Meth. Phys. Res. B **45**, 374 (1990)

[23] T.M. Thomas, H. Neumann, A.W. Czanderna and J.R. Pitts, Surf. Sci. **175**, L737 (1986)

[24] O.B. Firsov, Sov. Phys. JETP **36**, 1076 (1959)

[25] F. Shoji and T. Hanawa, Surf. Sci. **129**, L261 (1983)

[26] F. Shoji and T. Hanawa, Surf. Sci. **163**, L745 (1985)

[27] F. Shoji, Y. Nakayama, K. Oura and T. Hanawa, Nucl. Instr. Meth. Phys. Res. B **33**, 420 (1988)

[28] F. Shoji and T. Hanawa, Nucl. Instr. Meth. Phys. Res. B **2**, 401 (1984)

[29] G.C. van Leerdam, Ph.D. Thesis, Eindhoven University of Technology (1991)

[30] S.L.G. Toussaint, project report FOG-group, Eindhoven University of Technology (1993)

[31] H.B. Michaelson, J. Appl. Phys. **48**, 4729 (1977)

[32] R. Souda, T. Aizawa, C. Oshima and Y. Ishizawa, Nucl. Instr. Meth. Phys. Res. B **45**, 364 (1990)

[33] D.A. Papaconstantopoulos, *Handbook of the bandstructure of elemental solids* (Plenum Press, New York, 1986)

[34] Y. Muda and D.M. Newns, Phys. Rev. B **37** (12) 7048 (1988)

[35] Y. Muda and D.M. Newns, Nucl. Instr. Meth. Phys. Res. B **33**, 388 (1988)

[36] R. Souda, T. Aizawa, W. Hayami, S. Otani and Y. Ishizawa, Phys. Rev. B **42**, 7761 (1990)

[37] S.N. Mikhailov, L.C.A. van den Oetelaar and H.H. Brongersma, accepted for publication in Nucl. Instr. Meth. Phys. Res.

[38] S.N. Mikhailov, R.J.M. Elfrink, J.-P. Jacobs, L.C.A. van den Oetelaar, P.J. Scanlon and H.H. Brongersma, submitted to Nucl. Instr. Meth. Phys. Res.

[39] M. Barat and W. Lichten, Phys. Rev. A **6**, 211 (1972)

[40] C.C. Lu, T.A. Carlson, F.B. Malik, T.C. Tucker and C.W. Nestor, Atomic Data **3**, 1 (1971)

[41] D.P. Woodruff, Nucl. Instr. Meth. **194**, 639 (1982)

[42] M. Wuttig, W. Hoffmann, R.M. Jaeger, H. Kuhlenbeck and H.-J. Freund, Mat. Res. Soc. Symp. Proc. **221**, 143 (1991)

[43] S. Reijne, Master Thesis, Eindhoven University of Technology (1994)

[44] P. Novacek and P. Varga, Surf. Sci. **248**, 183 (1991)

[45] P.A.J. Ackermans, G.C.R. Krutzen and H.H. Brongersma, Nucl. Instr. Meth. Phys. Res. B **45**, 384 (1990)

[46] J.M. MacLaren, J.B. Pendry, P.J. Rous, D.K. Saldin, G.A. Somorjai, M.A. Van Hove and D.D. Vvedensky, *Surface Crystallographic Information Service* (D. Reidel Publishing Company, Dordrecht, 1987)

[47] A.G. Dirks and H.H. Brongersma, J. Electrochem. Soc. **127**, 2043 (1980)

[48] Eunjip Choi, S.-J. Oh and M. Choi, Phys. Rev. B **43**, 6360 (1991)

[49] S.-C. Lui, J.W. Davenport, E.W. Plummer, D.M. Zehner and G.W. Fernando Phys. Rev. B **42**, 1582 (1990)

[50] J.-P. Jacobs, S. Reijne, R.J.M. Elfrink, S.N. Mikhailov and H.H. Brongersma, submitted to J. Vac. Sci. Tech.

[51] *Electron tubes*, Philips Data handbook, part-9 (1980)

[52] H. van Benthem, Master Thesis, Eindhoven University of Technology (1994)

Appendix A

Detection system of the Mini-MOBIS

A schematic view of the detection system of the Mini-MOBIS is shown in figure A.1. The ions that pass the CMA are postaccelerated before they impinge on one of eight channeltrons (type B310BL [51]). The front of the channeltrons is kept at the same voltage as the postaccelaration (standard setting -100 V) whereas the back of the channeltrons is kept at +3500 V. The multiplied current pulse from the channeltrons is amplified in the pre-amp (Canberra 2004) and in the main amplifier (standard amplification factor 200). The pulse is counted if the pulse height (V) exceeds the discriminator level (standard setting 2.1 V).

The resistance of the eight channeltrons paralel is measured to be $\approx$ 750 MΩ. Due to an extra 100 MΩ resistor in the pre-amplifier, the real voltage between the front- and backside of the channeltrons is $\approx$ 3000 V (max. 4000 V [51]).

The pulses from the main amplifier have a width of $\approx 3\mu s$. The pulse height varies between 0 and 12.5 V (saturated level). The pulse- height distribution was measured using a Multi Channel Analyzer (MCA) in Pulse Height Analysis (PHA)-mode.

In figure A.2 PHA-spectra are plotted for 1, 2 and 3 keV He^+ incident on Cu. As one can see, the channeltrons are not in the saturated mode and the shape of the spectra is different at different incident energies. Furthermore, the lower level of the discriminator was set at 2.1 V, whereas the noise level is at $\approx$ 0.4 V. This means that only a fraction of

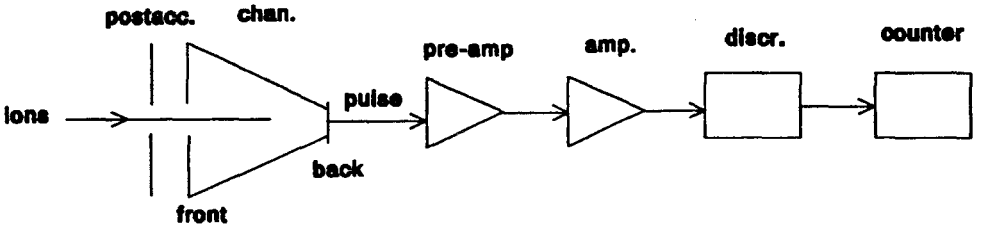

Figure A.1: Schematic view of the detection system of the Mini-MOBIS.

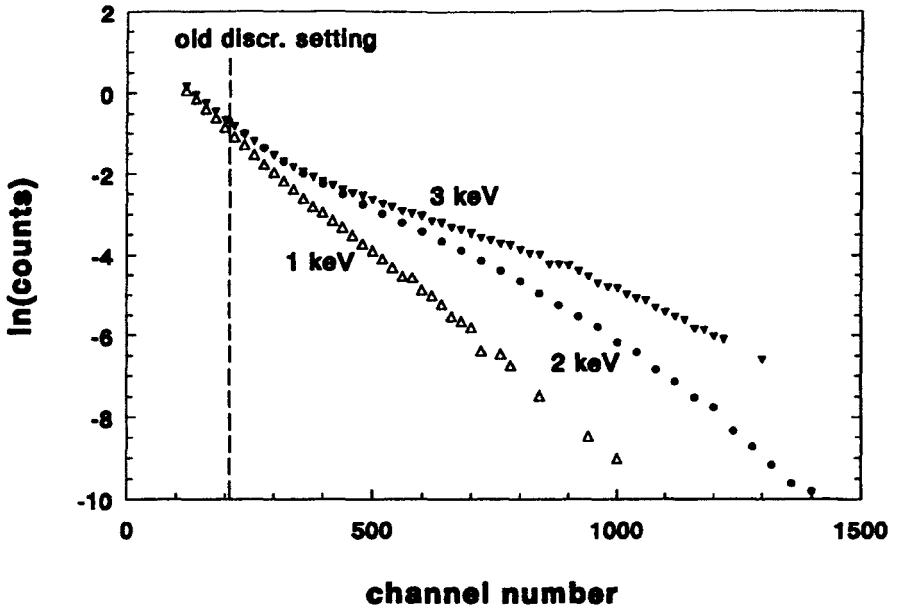

Figure A.2: PHA-spectra for 1, 2 and 3 keV He^+ incident on Cu.

the total 'real' counts is counted and that the counted fraction is energy dependent.

When PHA-spectra were measured from Cu and W at the same *final* energy, the shapes of the PHA-spectra were the same. This means that the counted fraction is *final*-energy dependent. For He^+-scattering, the ratio of the true number of counts and the counts above the old discriminator setting (2.1 V) is shown in figure A.3.

The efficiency of the channeltrons can vary with energy (or velocity) of the ions. An attempt was made to measure the efficiency by measuring the total number of counts in the PHA-spectra at different values for the postaccelaration and front of channeltron, while keeping the total voltage across the channeltrons constant. Within the errors, no change in total count was observed.

The results thus had to be corrected for the discriminator setting and (perhaps) also for a channeltron efficiency. For He^+-scattering both corrections are *final*-energy dependent. In the determination of the neutralization constant, (as in figure 4.7) it is thus better to plot $1/\sqrt{E_f}$ on the bottom axis in stead of $1/v_i + 1/v_f$, because then the correction is the same for all elements at a certain x-value (see figure A.4).

The straight line behavior, predicted from the theory, is found with good accuracy, which means that the final energy dependent correction (η) should have the form:

$$\eta = A \exp\left(\frac{-F}{\sqrt{E_f}}\right) \tag{A.1}$$

where F is a correction constant. Using $P^+ = \exp(-\lambda/\sqrt{E_f})$, where λ is the true neutralization constant, and using equation 2.2, the measured LEIS-intensity can be written

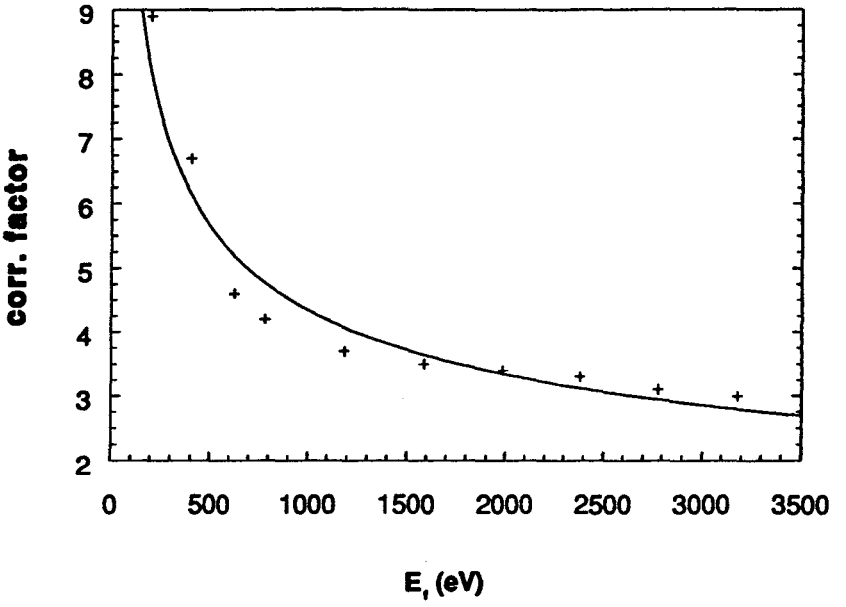

Figure A.3: Ratio of the total counts and counts above 2.1 V (old discriminator setting) as function of the final energy of the ion.

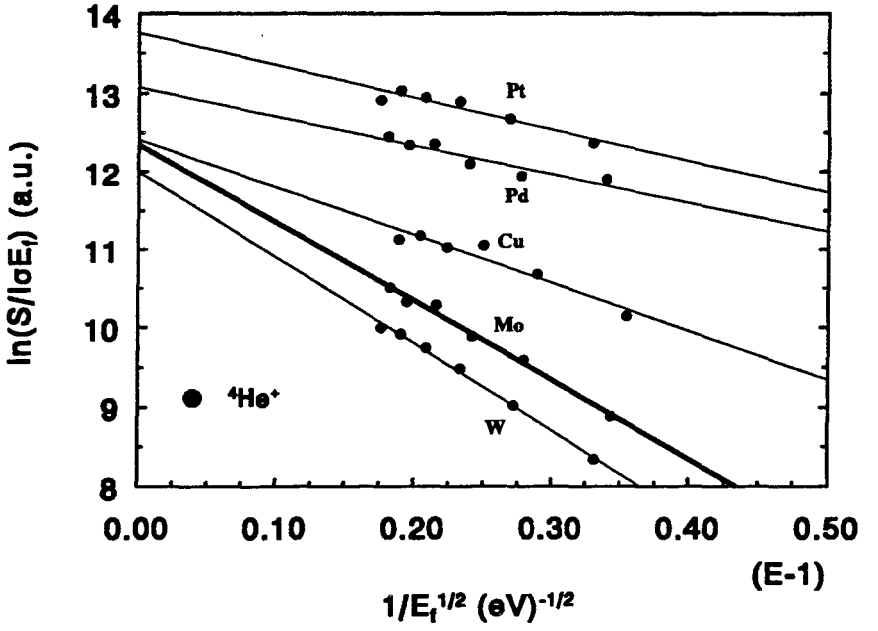

Figure A.4: Determination of a neutralization constant from a plot of $ln(S/\frac{d\sigma}{d\Omega}E_f)$ against ${E_f}^{-1/2}$. The correction at a certain x-value is now the same for all elements.

as:

$$S_i = cI_0 n_i \frac{d\sigma}{d\Omega} A \exp\left(\frac{-(F+\lambda)}{\sqrt{E_f}}\right) \tag{A.2}$$

and

$$\ln\left(\frac{S}{I_0 \frac{d\sigma}{d\Omega} E_f}\right) = D - \frac{M}{\sqrt{E_f}} \tag{A.3}$$

where D is a constant and $M = F + \lambda$ is the measured neutralization constant. If one element is taken as a reference element, we can write:

$$M - M^r = (\lambda + F) - (\lambda^r + F) = \lambda - \lambda^r \tag{A.4}$$

since the efficiency, represented by F, is the same for each element. This means that the differences of the *measured* neutralization constants (M) in a $1/\sqrt{E_f}$ -plot are the same as the differences of the *true* neutralization constants (λ).

Since

$$\frac{1}{v_i} + \frac{1}{v_f} = \frac{1}{\sqrt{2E_f/m_{He}}}(\sqrt{k}+1) \tag{A.5}$$

where k is the kinematic factor (E_f/E_i) for He^+-scattering from that element, equation A.4 can be converted to slopes in a $1/v_i + 1/v_f$ -plot (characteristic velocities v_c):

$$M(\sqrt{k}+1) - M^r(\sqrt{k_r}+1) = v_c(\sqrt{k}+1) - v_c^r(\sqrt{k_r}+1) \tag{A.6}$$

thus,

$$M - v_c = (M - v_c)^r \frac{(\sqrt{k_r}+1)}{(\sqrt{k}+1)} = \Gamma(M - v_c)^r \tag{A.7}$$

Since for most elements the value for Γ is between 0.9 and 1, as a first approximation, also in a $1/v$ plot the differences between the measured slopes are the same as the differences in the true characteristic velocities.

For a more detailed investigation on the detection system of the Mini-MOBIS see reference [52].

Appendix B

LEIS-spectra

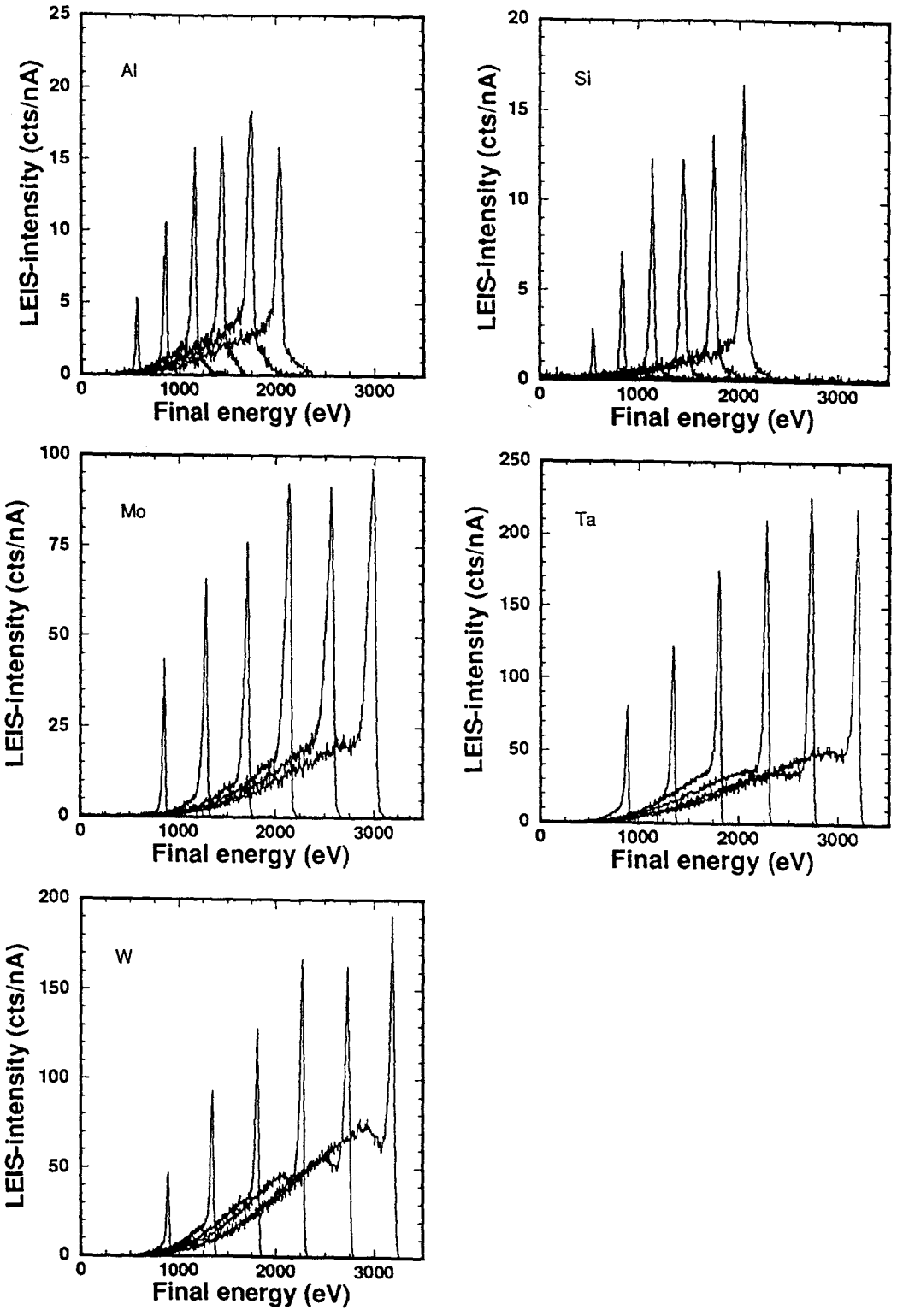

Figure B.1: LEIS-spectra using 1, 1.5, 2, 2.5, 3, 3.5 keV $^4He^+$ on different metals.

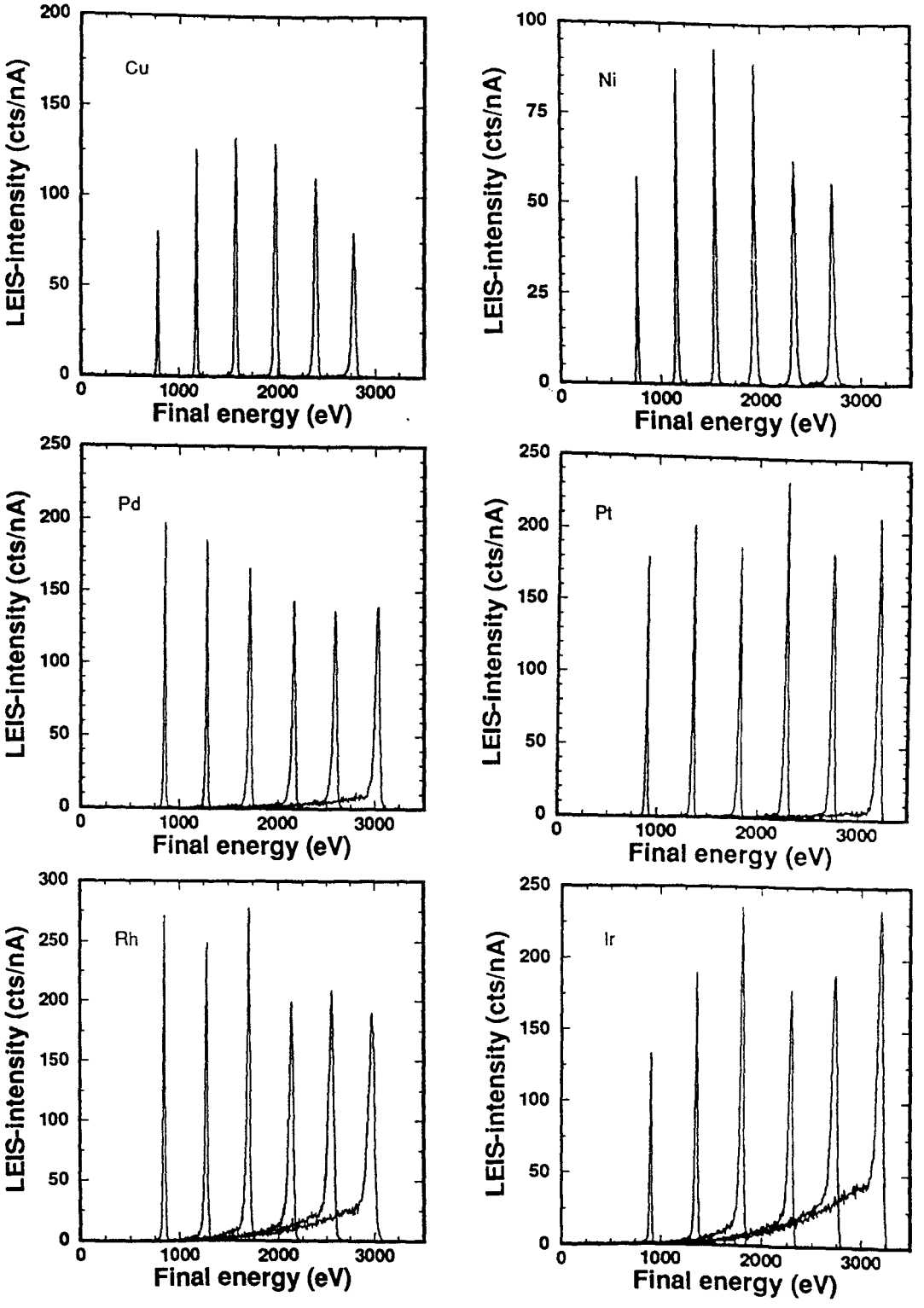

Figure B.2: LEIS-spectra using 1, 1.5, 2, 2.5, 3, 3.5 keV $^4He^+$ on different metals.

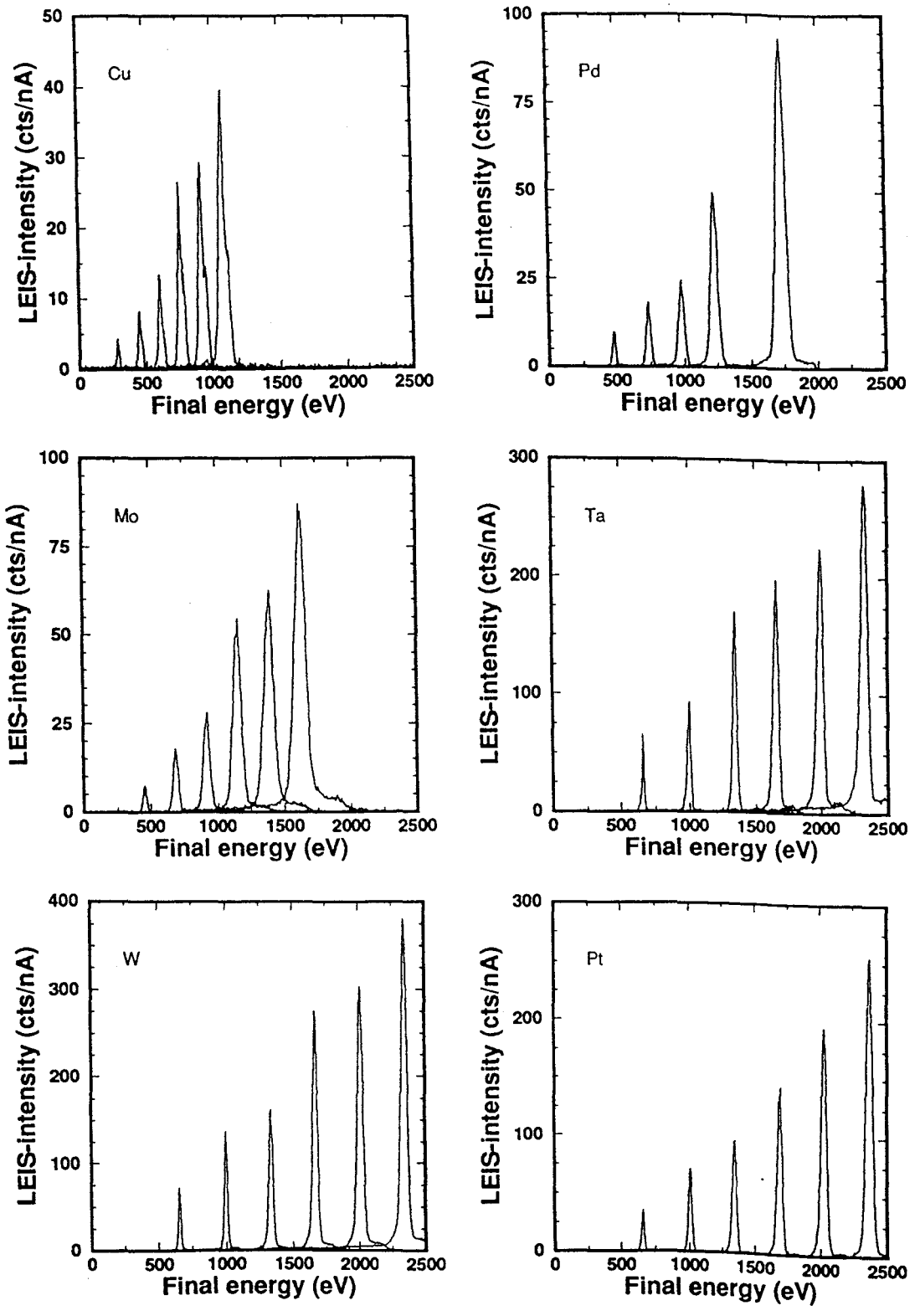

Figure B.3: LEIS-spectra using 1, 1.5, 2, 2.5, 3, 3.5 keV $^{20}Ne^{+}$ on different metals.

Appendix C

Low-Energy Ne^+-Scattering from Metals

In this appendix, the results of the experiments using Ne^+ as incident ion are shown. The structure of this chapter is the same as chapter four, where the He^+-results were presented.

C.1 Shape of LEIS-spectra

C.1.1 Reionization tails

Results

The LEIS spectra measured using Ne ions are also shown in appendix B. In table C.1 both threshold energy for reionization and tail to peak ratio are listed for the elements studied. As one can see from this table and from the spectra, the low-energy reionization tails are much less pronounced than in He^+ scattering. There are several reasons for this:

- the distance of closest approach is larger than for He^+ scattering (see figure 2.6). Since reionization occurs at small distances between ion and target (chapter 2), the probability for reionization for Ne^+ will be smaller than for He^+-scattering
- at the same kinetic energy, Ne ions have a much smaller velocity than He ions. Therefore, the probability for neutralization after reionization is much larger
- due to the higher mass, the energy after scattering for Ne^+ is smaller than for He^+ which again increases the probability for neutralization after reionization

C.1.2 Peak position

Results

The peak-shift data for Ne^+-scattering are presented in table C.2. As one can see, the inelastic energy-loss is of the same order as in He^+-scattering. Due to the fact that

element	E_{thr} (eV)	TP-ratio	element	E_{thr} (eV)	TP-ratio
Cu	—	—	Ta	500	0.03
Pd	1000	0.01	Mo	700	0.01
Pt	—	—	Ir	1400	0.01
W	—	—			

Table C.1: Threshold energies for reionization and TP-ratios for Ne^+ incident on the elements studied in this work. Due to the small reionization tails, the errors in E_{thr} are of the order of a few hundred eV. — means that no clear reionization tail is observed.

element	Q (eV) at			element	Q (eV) at		
	1 keV	2 keV	3 keV		1 keV	2 keV	3 keV
Cu	18	29	43	Mo	28	43	57
Pd	36	63		Ta	23	38	
W	31	38	48	Ir	33	49	70
Pt	42	52	75				

Table C.2: Peak shift of the LEIS surface-peak to lower energies for 1, 2 and 3 keV Ne^+ on different elements. The errors are ± 5 eV at 1 keV, ± 10 eV at 2 keV and ± 15 eV at 3 keV.

reionization-tails in Ne^+-spectra are not as pronounced as in He^+-scattering, the inelastic loss cannot be related to reionization. No satisfactory explanation can be given for the difference in inelastic loss for scattering from different targets.

C.1.3 FWHM of the surface peak

Results

In table C.3 the measured FWHM of 1, 2 and 3 keV Ne^+ incident on different elements are shown. The measured value for the FWHM is more or less the same for all elements, except for Mo and Pd which have much broader surface-peaks. A possible explanation for this is the large number of isotopes for Mo and Pd (table 4.4).

The FWHM-data cannot be related to reionization (as in the He^+-results), due to the fact that the reionization-tails for Ne^+-scattering are not as pronounced as for He^+-scattering.

element	FWHM (eV) at			element	FWHM (eV) at		
	1 keV	2 keV	3 keV		1 keV	2 keV	3 keV
Cu	18	30	46	Mo	31	54	83
Pd	25	50	-	Ta	17	37	-
W	19	33	46	Ir	22	35	53
Pt	19	35	50				

Table C.3: FWHM of LEIS surface-peaks for 1, 2 and 3 keV Ne^+ on different elements. The errors are ±5 eV at 1 keV, ±10 eV at 2 keV and ±15 eV at 3 keV.

C.2 Neutralization of primary ions

Results

The determination of v_c for Ne^+-scattering is shown in figure C.1.

As one can see, the linear relation, predicted by the theory of Hagstrum, is not observed. The data points can reasonably well be fitted with a second order polynomial. This might indicate that the neutralization parameter v_c is energy-dependent, as was proposed by O'Connor et al. [14].

Fitting of the data points of figure C.1 with a linear fit gives values for v_c between 1 and $3*10^5$ m/s.

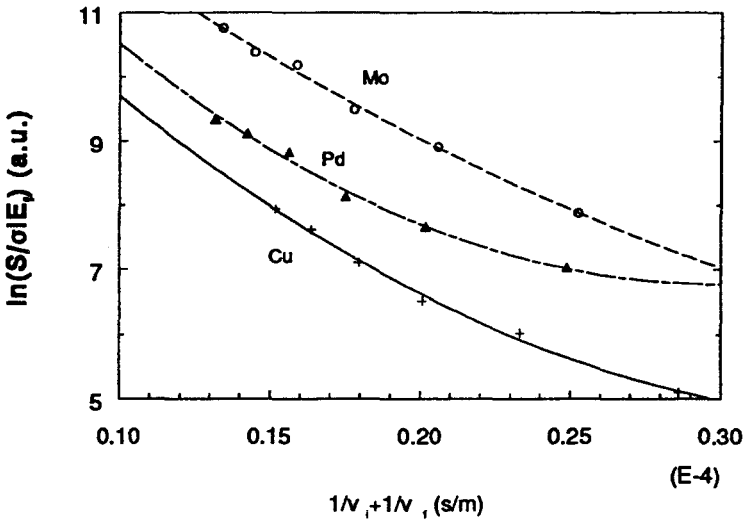

Figure C.1: Logarithm of LEIS-signal divided by cross section and final energy as function of the sum of the reicprocal velocities for Ne^+-scattering from different elements. The line is a second order polynomial fit to the data points.

Appendix D

Density of states of the studied elements

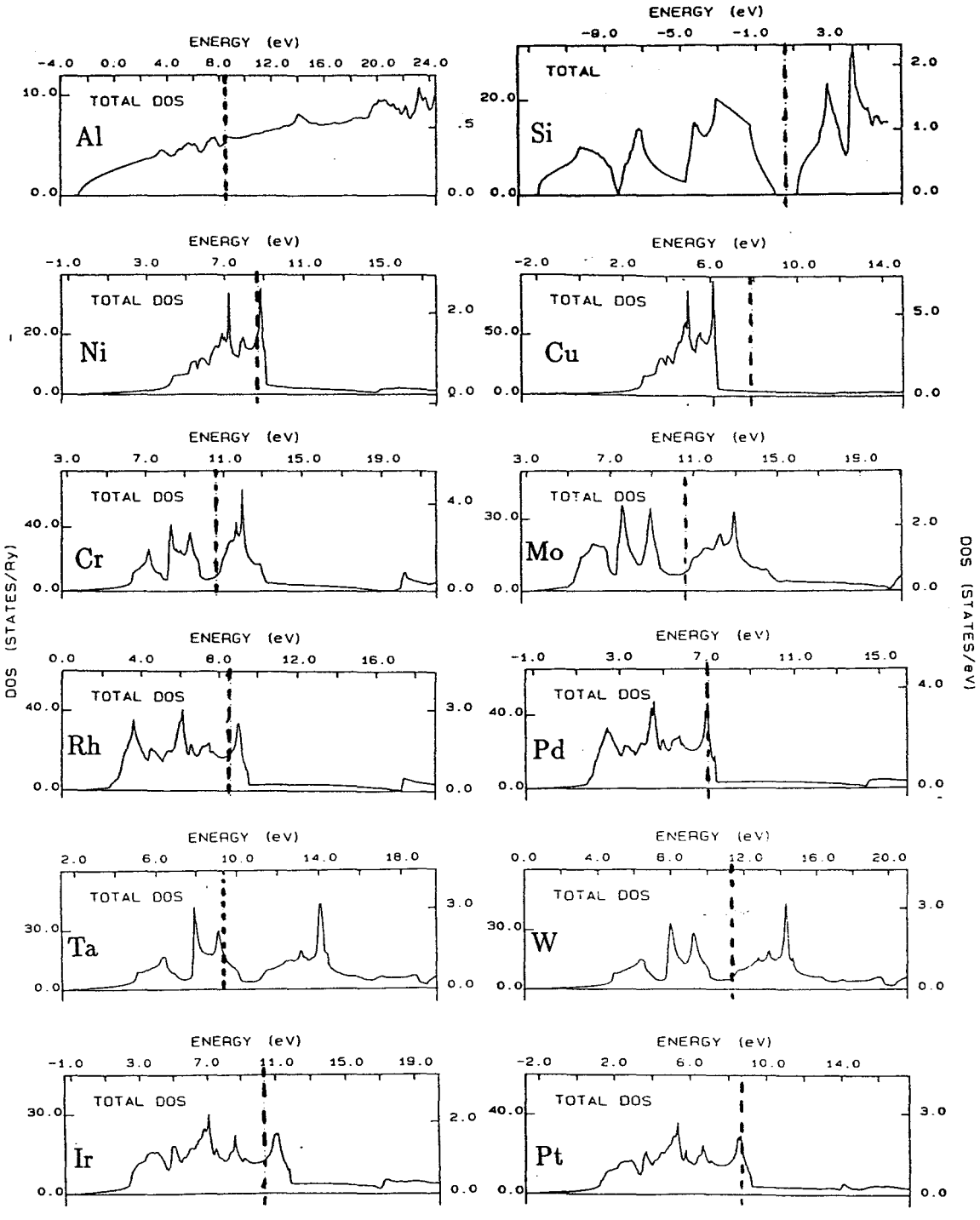

Figure D.1: Total electronic density of states of the pure elements studied in this work [33]. The dashed line indicates the Fermi-energy.